NASA Technical Memorandum 85655

Internal Pressure Distributions for a Two-Dimensional Thrust-Reversing Nozzle Operating at a Free-Stream Mach Number of Zero

Lawrence E. Putnam and Edward G. Strong

DECEMBER 1983

25th Anniversary
1958-1983

NASA

NASA Technical Memorandum 85655

Internal Pressure Distributions for a Two-Dimensional Thrust-Reversing Nozzle Operating at a Free-Stream Mach Number of Zero

Lawrence E. Putnam and Edward G. Strong
Langley Research Center
Hampton, Virginia

National Aeronautics
and Space Administration

**Scientific and Technical
Information Branch**

1983

SUMMARY

An investigation has been conducted in the static-test facility of the Langley 16-Foot Transonic Tunnel to measure static-pressure distributions inside a nonaxisymmetric thrust-reversing nozzle. The tests were made at nozzle total pressures ranging from ambient to about eight times ambient pressure at a free-stream Mach number of zero. Tabulated pressure data are presented. Results of the investigation show that the surface static pressures inside the nozzle are highly three-dimensional in character. The sonic line in the nozzle reverser port was highly inclined, causing significant losses in discharge coefficient.

INTRODUCTION

The mission requirements for the next generation of fighter airplanes will necessitate a highly versatile vehicle capable of operating over a wide range of flight conditions. The airplane will probably be required to have STOL (short take-off and landing) capabilities in order to operate from bomb-damaged airfields. According to reference 1, take-off and landing distances of less than 366 m are feasible if some form of propulsive lift or thrust reversing is used. In addition, the airplane will most likely be required to have maneuver capabilities equal to or greater than current fighter airplanes. However, the design and integration of the power plant and multifunction nozzles to provide these required capabilities is a difficult problem.

In recent years, many experimental studies have been made to determine static, low-speed, and flight performance of thrust-reversing nozzles. (See refs. 1 through 14, for example.) Both axisymmetric and nonaxisymmetric nozzle concepts have been studied. The primary benefit of the nonaxisymmetric nozzle is its versatility. Thrust-reversing and thrust-vectoring capabilities can be incorporated in this type nozzle with lower weight penalties than for conventional "round" nozzles. (See ref. 2.)

Although the large and expanding experimental data base provides overall performance characteristics of thrust-reverser nozzles, little is known about the flow inside the nozzle. The development of improved thrust-reverser concepts requires that an understanding of the flow phenomena inside the nozzle be developed. In addition, in order for the designer to be able to rapidly develop and assess new design concepts, accurate analytical methods must be developed to predict the flow inside the nozzle, and to predict the performance characteristics of thrust-reversing nozzles. The development of these analytical techniques also requires that the theoretician have an understanding of the flow processes inside the nozzle.

The purpose of the present investigation is, therefore, to provide detailed static-pressure measurements of the flow inside a two-dimensional convergent-divergent nozzle operating in the thrust-reversing mode. The nozzle configuration selected for the present investigation was one of several previously tested by Re and Leavitt (ref. 14) to obtain thrust- and discharge-coefficient data. The present investigation was conducted in the static-test facility of the Langley 16-Foot

Transonic Tunnel. The measurements were made at nozzle total-pressure ratios from jet off to about 8.0 with the free-stream Mach number equal to zero.

SYMBOLS

F	measured thrust along body axis
F_i	ideal isentropic gross thrust (see ref. 14)
p	local static pressure
p_a	ambient pressure
$p_{t,j}$	jet total pressure
s	axial coordinate (see fig. 2)
t	vertical coordinate (see fig. 2)
w_i	ideal isentropic weight flow (see ref. 14)
w_p	measured weight flow
x	coordinate parallel to blocker face (see figs. 5(b) and 5(c))
y	coordinate perpendicular to nozzle sidewall (see fig. 5(a))
z	coordinate perpendicular to blocker face (see fig. 5(c))

Abbreviations

NPR	nozzle total-pressure ratio, $p_{t,j}/p_a$
Sta	station
2-D	two-dimensional, as in 2-D nozzle (in reality, the 2-D nozzle is rectangular)

APPARATUS AND METHODS

Static-Test Facility

This investigation was conducted in the static-test facility of the Langley 16-Foot Transonic Tunnel. The testing was done in a room where the jet could exhaust to atmosphere through an open doorway. This facility utilizes the same clean, dry-air supply as that used in the Langley 16-Foot Transonic Tunnel and a similar air-control system, including valving, filters, and a heat exchanger (to operate the jet flow at constant stagnation temperature). Data taken in this facility are recorded on the Langley 16-Foot Transonic Tunnel 128-channel, magnetic-tape data acquisition system. More details of this data acquisition system are in reference 15.

Single-Engine Propulsion Simulation System

Figure 1 is a sketch of the single-engine, air-powered, propulsion simulation system on which various nozzles can be mounted for testing in the static-test facility. This propulsion simulation system, which is also used in the Langley 16-Foot Transonic Tunnel, is described in detail in reference 15. For tests in the static-test facility, the body shell forward of station (Sta.) 52.07 cm is removed.

An external high-pressure air system provided a continuous flow of clean, dry air at a controlled temperature of about 300 K. This air, at pressures up to approximately 8 atm (1 atm = 101.3 kPa), was brought through a dolly-mounted support strut by six tubes which connect to a high-pressure plenum chamber. As shown in figure 1, the air was then discharged into the model low-pressure plenum normal to the model axis through eight multiholed sonic nozzles equally spaced around the high-pressure plenum. This air injection method was designed to minimize any forces imposed by the transfer of axial momentum as the air is passed from the nonmetric high-pressure plenum to the metric (mounted to a force balance) low-pressure plenum. Two flexible metal bellows are used as seals and serve to compensate for axial forces caused by pressurization.

The air was then passed from the low-pressure plenum (circular in cross section) through a transition section, choke plate, and instrumentation section. The transition section provided a smooth flow path for the airflow from the round low-pressure plenum to the rectangular choke plate and instrumentation section. The instrumentation section had a flow-path width-to-height ratio of 1.437 and was identical in geometry to the nozzle airflow entrance. The nozzle was attached to the instrumentation section at model station 104.47 cm.

2-D Thrust-Reverser Nozzle

A sketch providing details of the 2-D thrust-reverser nozzle is presented as figure 2, and figures 3 and 4 are photographs of the nozzle configuration. This thrust-reverser nozzle is configuration R2 of reference 14 and is representative of the thrust-reverser arrangement for all the dry-power, 2-D, convergent-divergent nozzles tested in reference 14. The reverser port of the 2-D, thrust-reversing nozzle used in the present investigation was inclined forward 30° and had a throat aspect ratio of 6.084. The internal width of this rectangular nozzle was 10.160 cm.

Instrumentation

Jet total pressure was measured at a fixed station in the instrumentation section (see fig. 1) by means of a four-probe rake through the upper surface, a three-probe rake through the side, and a three-probe rake through the corner. The nozzle pressure ratio (NPR) was determined by averaging these measurements. A thermocouple, also located in the instrumentation section, was used to measure jet total temperature. Sixteen internal static-pressure orifices were located on the nozzle flap in the reverser port. (See figs. 3 and 5(a).) Twelve static-pressure orifices were located on the internal surface of the flap. (See fig. 5(a).) Thirty-six static-pressure orifices were located on the blocker (fig. 5(b)), and 60 static-pressure orifices were located on the sidewall (figs. 4 and 5(c)). Coordinates of the static-pressure orifice locations are given in table I.

Test Procedure

Data were obtained in the static-test facility at static conditions (free-stream Mach number of 0). The ratio of jet total pressure to free-stream ambient pressure NPR was varied from jet off (NPR = 1.0) to approximately 8.0. The stagnation temperature of the jet flow was held at approximately 300 K.

Data Reduction

All data were recorded on magnetic tape using the Langley 16-Foot Transonic Tunnel data acquisition system. At each test point, approximately 50 samples of data were recorded at a rate of 10 samples per second. The samples were averaged, and the averaged values were used for all computations.

RESULTS AND DISCUSSION

Internal static-pressure data are presented in table II. Typical internal static-pressure distributions are presented in figures 6 through 11. Thrust- and discharge-coefficient data measured by Re and Leavitt (ref. 14) are presented as a function of nozzle pressure ratio in figure 12.

The effects of nozzle pressure ratio (NPR) on the static pressures on the nozzle sidewall are shown in figure 6. In general, it can be seen that there are only small effects of NPR on the sidewall pressures until x exceeds approximately 4.5 cm, which is well up into the reverser port. This sensitivity to NPR occurs primarily in regions of the nozzle where the flow is supersonic (i.e., where $p/p_{t,j}$ is less than 0.5283). There is also a significant variation of the static pressure across the reverser port on the sidewall. (See figs. 7 and 8.) At values of x greater than approximately 3.5 cm, the sidewall pressures change with both z and NPR. The large differences in static pressure are associated with the rapid turning of the flow around the flap lip. As can be seen in figure 8, however, upstream of the blocker face about 2 cm, where the velocity is very low (i.e., where $p/p_{t,j}$ is close to one) there is very little effect of NPR or spatial location on the sidewall pressures.

Figure 9 is a contour plot of the static pressures on the nozzle sidewall for a nozzle pressure ratio of 5.0. Re and Leavitt in reference 14 show that discharge coefficient w_p/w_i for this thrust-reversing nozzle varies significantly with nozzle pressure ratio up to 3.0 and is very low at nozzle pressure ratios above 3.0. (See fig. 12.) The low discharge coefficients for nozzle pressure ratios above 3.0 may be associated with flow nonuniformity. This nonuniformity is indicated by the highly inclined sonic line shown in the pressure contours on the sidewall. (See fig. 9.) The low discharge coefficient may also be associated with flow separation due to the 120° turn around the sharp lip. The failure of the pressures at $z = 1.473$ on the sidewall (fig. 7) to continue to decrease beyond $x \approx 5.0$ cm at NPR = 2.0 and 3.0 is evidence that separation may have occurred. Also, there are indications of a strong shock (fig. 6(b)) at $x \approx 5.5$ cm in the center of the reverser port. This shock wave may also be responsible for the low discharge coefficients.

The three dimensionality of the flow in the reverser port is evident from the blocker-face pressure distributions shown in figure 10 and from the pressure distributions on the flap in the reverser port shown in figure 11. There is a small region of essentially constant pressure near the reverser-port centerline. However, as the

sidewall is approached, the flow becomes very three-dimensional in character. These results have strong implications for the development of theoretical methods for predicting thrust-reverser performance. Theoretical calculations of the flow in 2-D nozzles operating in the normal forward-thrust mode have shown that as long as the nozzle sidewalls are essentially parallel, 2-D analytical methods can be used to provide a reasonable estimate of the nozzle flow. (See refs. 16 and 17, for example.) However, the results of the present investigation indicate that any method developed to compute the detailed flow in a 2-D nozzle operating in the reverse-thrust mode needs to account for the three-dimensionality of the flow.

CONCLUSION

An investigation has been conducted in the static-test facility of the Langley 16-Foot Transonic Tunnel to measure the static pressure inside a two-dimensional thrust-reversing nozzle. The tests were made with one nozzle configuration operating at nozzle pressure ratios from jet-off to about 8.0. Free-stream Mach number was zero. The results of the investigation showed significant three-dimensional variations of the pressure in the reverser port. This nozzle configuration had a highly inclined sonic line and evidence of separated flow at nozzle pressure ratios below 3.0. As a result, the nozzle had a very low discharge coefficient at all nozzle pressure ratios. From the variations in the surface pressures shown in this investigation, it is most likely that theoretical methods developed to predict the flow characteristics of thrust-reversing nozzles will have to be three-dimensional.

Langley Research Center
National Aeronautics and Space Administration
Hampton, VA 23665
October 21, 1983

REFERENCES

1. Capone, Francis J.; Re, Richard J.; and Bare, E. Ann: Thrust Reversing Effects on Twin-Engine Aircraft Having Nonaxisymmetric Nozzles. AIAA-81-2639, Dec. 1981.

2. Wallace, Hoyt W.; and Bowers, Douglas L.: Advanced Nozzle Integration for Air Combat Fighter Application. AIAA-82-1135, June 1982.

3. Mercer, Charles E.; and Maiden, Donald L.: Effects of an In-Flight Thrust Reverser on the Stability and Control Characteristics of a Single-Engine Fighter Airplane Model. NASA TN D-6886, 1972.

4. Goetz, Gerald F.; Young, John H.; and Palcza, J. Lawrence: A Two-Dimensional Airframe Integrated Nozzle Design With Inflight Thrust Vectoring and Reversing Capabilities for Advanced Fighter Aircraft. AIAA Paper No. 76-626, July 1976.

5. Capone, Francis J.; and Maiden, Donald L.: Performance of Twin Two-Dimensional Wedge Nozzles Including Thrust Vectoring and Reversing Effects at Speeds up to Mach 2.20. NASA TN D-8449, 1977.

6. Capone, Francis J.: Static Performance of Five Twin-Engine Nonaxisymmetric Nozzles With Vectoring and Reversing Capability. NASA TP-1224, 1978.

7. Capone, Francis J.; and Berrier, Bobby L.: Investigation of Axisymmetric and Nonaxisymmetric Nozzles Installed on a 0.10-Scale F-18 Prototype Airplane Model. NASA TP-1638, 1980.

8. Bare, E. Ann; Berrier, Bobby L.; and Capone, Francis J.: Effects of Simulated In-Flight Thrust Reversing on Vertical-Tail Loads of F-18 and F-15 Airplane Models. NASA TP-1890, 1981.

9. Lorincz, Dale J.; Chiarelli, Charles; and Hunt, Brian L.: Effect of In-Flight Thrust Reverser Deployment on Tactical Aircraft Stability and Control. AIAA-81-1446, July 1981.

10. Blackman, J. P.; and Eigenmann, M. F.: Axisymmetric Approach and Landing Thrust Reversers. AIAA-81-1650, Aug. 1981.

11. Re, Richard J.; and Berrier, Bobby L.: Static Internal Performance of Single Expansion-Ramp Nozzles With Thrust Vectoring and Reversing. NASA TP-1962, 1982.

12. Leavitt, Laurence D.; and Re, Richard J.: Static Internal Performance Characteristics of Two Thrust-Reverser Concepts for Axisymmetric Nozzles. NASA TP-2025, 1982.

13. Capone, Francis J.; Mason, Mary L.; and Carson, George T., Jr.: Thrust Reversing Effects on Horizontal Tail Effectiveness of Twin-Engine Fighter Aircraft. AIAA-83-0086, Jan. 1983.

14. Re, Richard J.; and Leavitt, Laurence D.: Static Internal Performance Including Thrust Vectoring and Reversing of Two-Dimensional Convergent-Divergent Nozzles. NASA TP-2253, 1984.

15. Peddrew, Kathryn H., compiler: A User's Guide to the Langley 16-Foot Transonic Tunnel. NASA TM-83186, 1981.

16. Mason, Mary L.; Putnam, Lawrence E.; and Re, Richard J.: The Effect of Throat Contouring on Two-Dimensional Converging-Diverging Nozzles at Static Conditions. NASA TP-1704, 1980.

17. Swanson, R. C.: Navier-Stokes Solutions for Nonaxisymmetric Nozzle Flows. AIAA-81-1217, June 1981.

TABLE I.- INTERNAL STATIC-PRESSURE ORIFICE LOCATIONS

(a) Sidewall (See fig. 5(c))

x, cm	z, cm								
	0.203	0.381	0.838	1.473	2.108	2.743	3.378	4.013	4.648
0.218		X							
.485			X						
.851				X					
1.217					X				
1.245	X		X	X					
1.585						X			
1.880	X		X	X					
1.951							X		
2.515	X		X	X	X	X	X	X	
2.685									X
3.150	X		X	X	X	X	X	X	X
3.658	X		X	X	X	X	X	X	
4.166	X		X	X	X	X	X	X	
4.674	X		X	X	X	X	X	X	
5.182	X		X	X		X	X		
5.690	X		X	X					
6.198			X	X					
6.706				X					

TABLE I.- Concluded

(b) Blocker (see fig. 5(b))

x, cm	y, cm			
	0.635	1.905	3.493	5.080
0.098	X	X	X	X
1.245	X	X	X	X
1.880	X	X	X	X
2.515	X	X	X	X
3.150	X	X	X	X
3.658	X	X	X	X
4.166	X	X	X	X
4.674	X	X	X	X
5.182	X	X	X	X

(c) Flap reverser port surface (see fig. 5(a))

x, cm	y, cm			
	0.635	1.905	3.493	5.080
5.182	X	X	X	X
5.690	X	X	X	X
6.198	X	X	X	X
6.706	X	X	X	X

(d) Flap internal surface (see fig. 5(a))

x, cm	z, cm	y, cm			
		0.635	1.905	3.493	5.080
5.024	2.108	X	X	X	X
5.299	2.585	X	X	X	X
5.574	3.062	X	X	X	X

TABLE II.- INTERNAL STATIC PRESSURES

(a) Blocker static-pressure ratio $p/p_{t,j}$

NPR	$p/p_{t,j}$ at x, cm, of -								
	0.098	1.245	1.880	2.515	3.150	3.658	4.166	4.674	5.182
y = 0.635 cm									
1.0	1.004	1.000	1.000	1.003	1.002	1.001	1.000	1.001	1.001
2.0	1.003	.997	.996	.990	.965	.935	.868	.766	.615
3.0	1.003	.997	.996	1.003	.996	.927	.850	.742	.582
4.0	1.004	.998	.996	.989	.960	.924	.846	.736	.576
5.0	1.004	.999	.996	.988	.960	.921	.844	.732	.572
6.0	1.004	1.000	.997	.987	.960	.920	.844	.729	.571
7.0	1.002	1.000	.996	.986	.960	.919	.844	.728	.570
8.0	1.000	.999	.996	.984	.960	.918	.844	.727	.570
y = 1.905 cm									
1.0	1.004	1.004	0.998	1.004	1.004	1.001	1.002	1.001	
2.0	1.001	1.002	1.000	.996	.987	.966	.921	.829	
3.0	1.001	1.002	1.000	1.001	1.002	.964	.914	.810	
4.0	1.002	1.003	.999	.997	.987	.964	.915	.811	
5.0	1.003	1.003	.999	.998	.987	.965	.917	.812	
6.0	1.003	1.002	1.000	.997	.987	.965	.916	.812	
7.0	1.001	1.000	.999	.997	.986	.964	.916	.812	
8.0	.999	.998	.999	.994	.984	.963	.915	.812	
y = 3.493 cm									
1.0	1.005	1.000	0.999	1.005	0.998	1.002	0.999	1.001	1.002
2.0	1.002	1.001	.999	.999	.988	.968	.918	.828	.679
3.0	1.002	1.001	.999	1.003	1.000	.965	.906	.807	.644
4.0	1.004	1.001	1.000	1.000	.986	.965	.906	.807	.643
5.0	1.004	1.002	1.000	1.000	.987	.965	.907	.807	.644
6.0	1.004	1.003	1.001	1.000	.987	.964	.907	.807	.644
7.0	1.003	1.002	1.000	.999	.986	.963	.906	.807	.644
8.0	1.001	1.001	.999	.997	.985	.962	.906	.806	.644
y = 5.080 cm									
1.0	1.002	1.005	0.995	1.000	1.005	1.000	1.004	1.000	
2.0	.997	1.001	1.002	.992	.985	.959	.912	.815	
3.0	.997	1.001	1.002	.996	1.001	.954	.902	.792	
4.0	.997	1.002	1.000	.992	.985	.954	.902	.791	
5.0	.999	1.002	1.001	.993	.985	.955	.902	.792	
6.0	.999	1.002	1.000	.993	.984	.954	.902	.792	
7.0	.998	1.001	.999	.993	.984	.953	.901	.792	
8.0	.997	.999	.999	.991	.982	.953	.901	.792	

TABLE II.- Continued

(b) Flap upper-surface static pressure

NPR	$p/p_{t,j}$ at x, cm, of -				NPR	$p/p_{t,j}$ at x, cm, of -			
	5.182	5.690	6.198	6.706		5.182	5.690	6.198	6.706
y = 0.635 cm					y = 1.905 cm				
1.0	1.002	1.000	1.000	1.001	1.0	1.005	1.000	1.002	1.001
2.0	.324	.339	.431	.521	2.0	.349	.340	.380	.473
3.0	.175	.265	.356	.384	3.0	.202	.197	.315	.421
4.0	.168	.265	.351	.326	4.0	.195	.191	.319	.413
5.0	.166	.266	.348	.325	5.0	.193	.190	.320	.410
6.0	.164	.267	.346	.324	6.0	.191	.189	.320	.407
7.0	.163	.268	.344	.322	7.0	.190	.188	.320	.406
8.0	.162	.268	.341	.320	8.0	.187	.187	.319	.404
y = 3.493 cm					y = 5.080 cm				
1.0	1.006	0.998	1.002	1.002	1.0	1.000	1.001	1.000	1.001
2.0	.367	.362	.377	.423	2.0	.368	.362	.378	.427
3.0	.212	.208	.266	.346	3.0	.213	.208	.269	.345
4.0	.205	.200	.269	.346	4.0	.204	.199	.275	.345
5.0	.204	.197	.273	.346	5.0	.202	.198	.279	.344
6.0	.202	.196	.275	.345	6.0	.200	.196	.281	.343
7.0	.201	.194	.276	.344	7.0	.198	.196	.281	.342
8.0	.200	.193	.275	.342	8.0	.197	.195	.281	.341

(c) Flap lower-surface static pressure

NPR	$p/p_{t,j}$ at x, cm, of -			NPR	$p/p_{t,j}$ at x, cm, of -		
	5.024	5.299	5.574		5.024	5.299	5.574
y = 0.635 cm				y = 1.905 cm			
1.0	0.999	1.002	0.989	1.0	0.992	0.994	1.000
2.0	.955	.959	.971	2.0	.943	.958	.962
3.0	.948	.954	.963	3.0	.933	.950	.957
4.0	.946	.954	.961	4.0	.932	.949	.955
5.0	.945	.955	.961	5.0	.931	.950	.956
6.0	.944	.956	.959	6.0	.931	.949	.955
7.0	.943	.958	.959	7.0	.931	.949	.955
8.0	.941	.957	.957	8.0	.930	.949	.953
y = 3.493 cm				y = 5.080 cm			
1.0	0.993	0.996	0.991	1.0	0.987	0.999	1.002
2.0	.941	.954	.961	2.0	.946	.955	.955
3.0	.931	.946	.954	3.0	.936	.948	.950
4.0	.931	.946	.953	4.0	.935	.947	.950
5.0	.931	.946	.954	5.0	.934	.948	.951
6.0	.930	.946	.953	6.0	.933	.948	.951
7.0	.931	.946	.953	7.0	.933	.947	.951
8.0	.930	.945	.953	8.0	.932	.945	.949

TABLE II.- Continued

(d) Sidewall static pressure

NPR	$p/p_{t,j}$ at x, cm, of -										
	1.245	1.880	2.515	3.150	3.658	4.166	4.674	5.182	5.690	6.198	6.706
z = 0.203 cm											
1.0	0.999	0.999	1.000	0.998	1.000	0.999	1.002	1.015	1.001		
2.0	1.002	.997	.988	.969	.934	.871	.781	.651	.501		
3.0	1.002	.997	1.001	.996	.926	.858	.763	.624	.447		
4.0	1.002	.997	.986	.964	.927	.859	.763	.624	.445		
5.0	1.002	.997	.986	.964	.927	.861	.764	.623	.446		
6.0	1.002	.997	.986	.964	.927	.861	.765	.622	.450		
7.0	1.001	.997	.985	.963	.927	.862	.765	.621	.444		
8.0	1.000	.996	.985	.962	.927	.861	.765	.620	.444		
z = 0.838 cm											
1.0	1.005	1.000	0.998	0.998	1.000	0.999	1.004	1.002	1.000	1.001	
2.0	1.001	.995	.984	.957	.915	.864	.761	.502	.398	.423	
3.0	1.001	.995	.998	.993	.903	.857	.741	.334	.344	.235	
4.0	1.001	.993	.974	.948	.904	.862	.742	.250	.342	.225	
5.0	1.001	.993	.973	.949	.905	.867	.742	.200	.340	.223	
6.0	1.001	.994	.971	.951	.904	.869	.742	.167	.339	.221	
7.0	1.000	.993	.971	.952	.903	.870	.742	.143	.338	.220	
8.0	.998	.993	.969	.952	.903	.871	.742	.125	.338	.219	
z = 1.473 cm											
1.0	1.001	0.998	0.998	0.997	0.998	0.996	1.004	0.999	1.001	1.001	1.003
2.0	.994	.983	.963	.954	.954	.921	.684	.331	.337	.442	.539
3.0	.994	.983	.971	.978	.951	.911	.640	.202	.241	.343	.385
4.0	.990	.976	.960	.960	.952	.910	.640	.207	.247	.334	.306
5.0	.989	.975	.962	.963	.954	.910	.640	.210	.252	.331	.293
6.0	.990	.975	.963	.965	.953	.909	.641	.210	.254	.326	.287
7.0	.989	.973	.964	.965	.953	.908	.641	.209	.256	.322	.283
8.0	.988	.973	.963	.964	.953	.907	.644	.208	.255	.319	.281

TABLE II.- Continued

(d) Continued

NPR	$p/p_{t,j}$ at x, cm, of -					
	2.515	3.150	3.658	4.166	4.674	5.182
z = 2.108						
1.0	0.997	0.997	0.998	0.998	1.007	
2.0	.979	.977	.968	.961	.959	
3.0	.983	1.002	.963	.957	.954	
4.0	.979	.976	.964	.958	.953	
5.0	.980	.976	.965	.957	.953	
6.0	.980	.976	.964	.957	.953	
7.0	.980	.975	.964	.956	.952	
8.0	.980	.974	.964	.955	.951	
z = 2.743 cm						
1.0	0.995	1.005	0.995	1.002	0.997	1.002
2.0	.985	.978	.977	.970	.963	.966
3.0	1.000	1.000	.974	.969	.961	.962
4.0	.982	.977	.974	.969	.962	.962
5.0	.982	.977	.974	.969	.962	.963
6.0	.982	.976	.974	.968	.963	.963
7.0	.981	.976	.973	.968	.965	.962
8.0	.980	.974	.973	.967	.963	.961
z = 3.378 cm						
1.0	1.002	1.000	0.999	1.000	1.003	1.005
2.0	.979	.980	.975	.971	.970	.968
3.0	.999	.991	.972	.968	.966	.964
4.0	.979	.978	.973	.969	.966	.964
5.0	.980	.980	.974	.971	.966	.964
6.0	.980	.980	.975	.970	.967	.964
7.0	.981	.979	.975	.970	.966	.963
8.0	.979	.979	.974	.969	.966	.963

TABLE II.- Continued

(d) Concluded

NPR	$p/p_{t,j}$ at x, cm, of -					
	2.515	3.150	3.658	4.166	4.674	3.150
	z = 4.013 cm					z = 4.648 cm
1.0	0.996	1.001	0.998	1.001	1.002	1.002
2.0	.982	.979	.975	.972	.970	.973
3.0	.999	.960	.972	.969	.966	.971
4.0	.979	.978	.973	.970	.967	.972
5.0	.980	.978	.974	.972	.967	.974
6.0	.980	.978	.974	.971	.967	.974
7.0	.980	.978	.974	.971	.967	.974
8.0	.979	.977	.974	.971	.967	.973

TABLE II.- Concluded

(e) Sidewall centerline static pressure

NPR	$p/p_{t,j}$ at (x,z), cm, of -						
	$\binom{0.219}{0.380}$	$\binom{0.484}{0.838}$	$\binom{0.851}{1.473}$	$\binom{1.217}{2.108}$	$\binom{1.584}{2.743}$	$\binom{1.950}{3.378}$	$\binom{2.684}{4.648}$
1.0	1.002	1.000	0.999	0.998	0.998	0.999	0.998
2.0	.967	1.002	1.001	.977	.985	.982	.980
3.0	.967	1.002	1.001	.977	.985	.995	.978
4.0	.958	1.002	.996	.970	.984	.980	.978
5.0	.958	1.003	.995	.970	.985	.981	.979
6.0	.958	1.003	.994	.971	.986	.981	.978
7.0	.957	1.003	.991	.971	.985	.981	.976
8.0	.957	1.002	.990	.970	.985	.980	.975

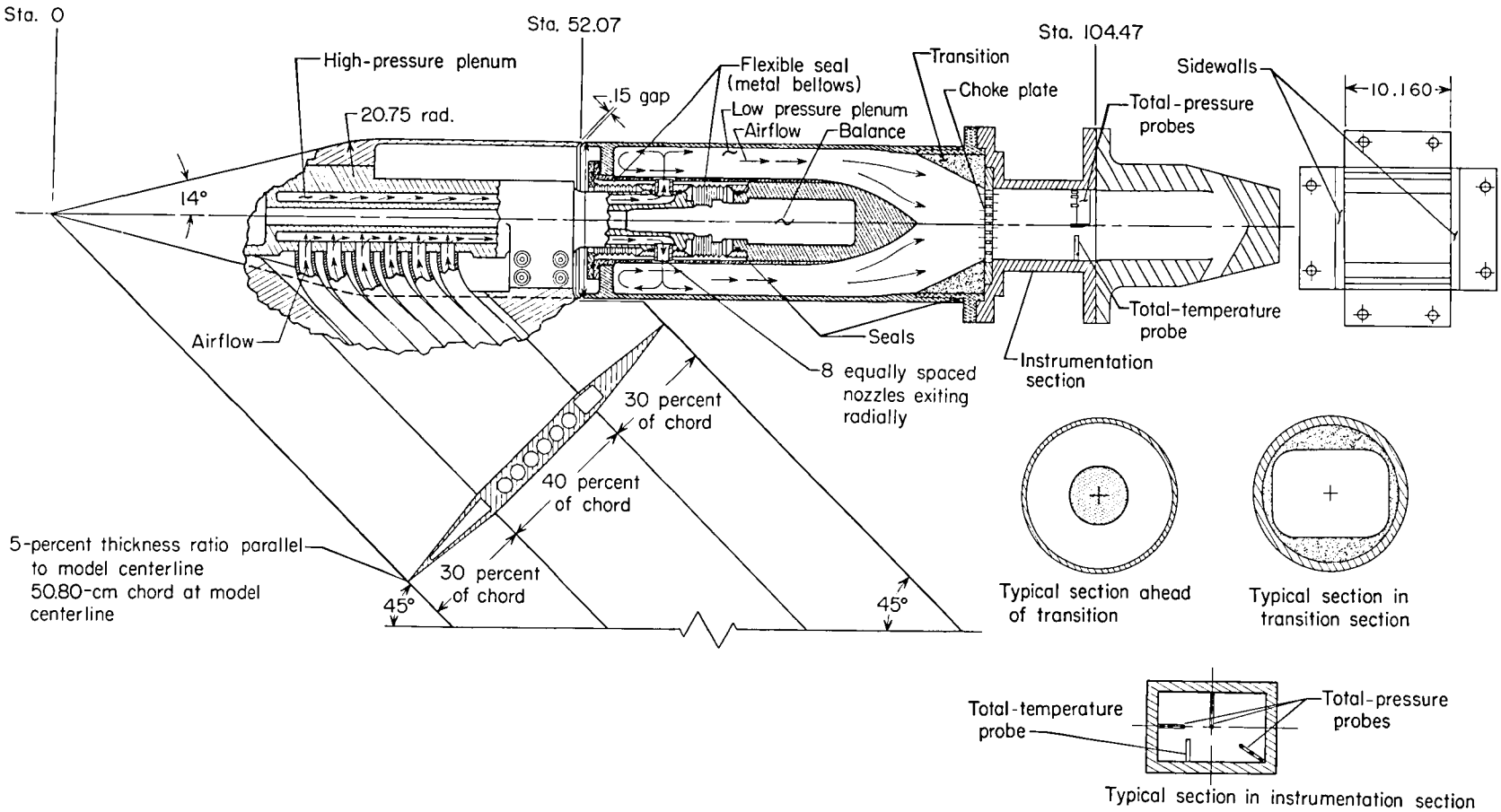

Figure 1.- Sketch of air-powered nacelle model with nozzle configuration installed. All dimensions are in centimeters unless otherwise noted.

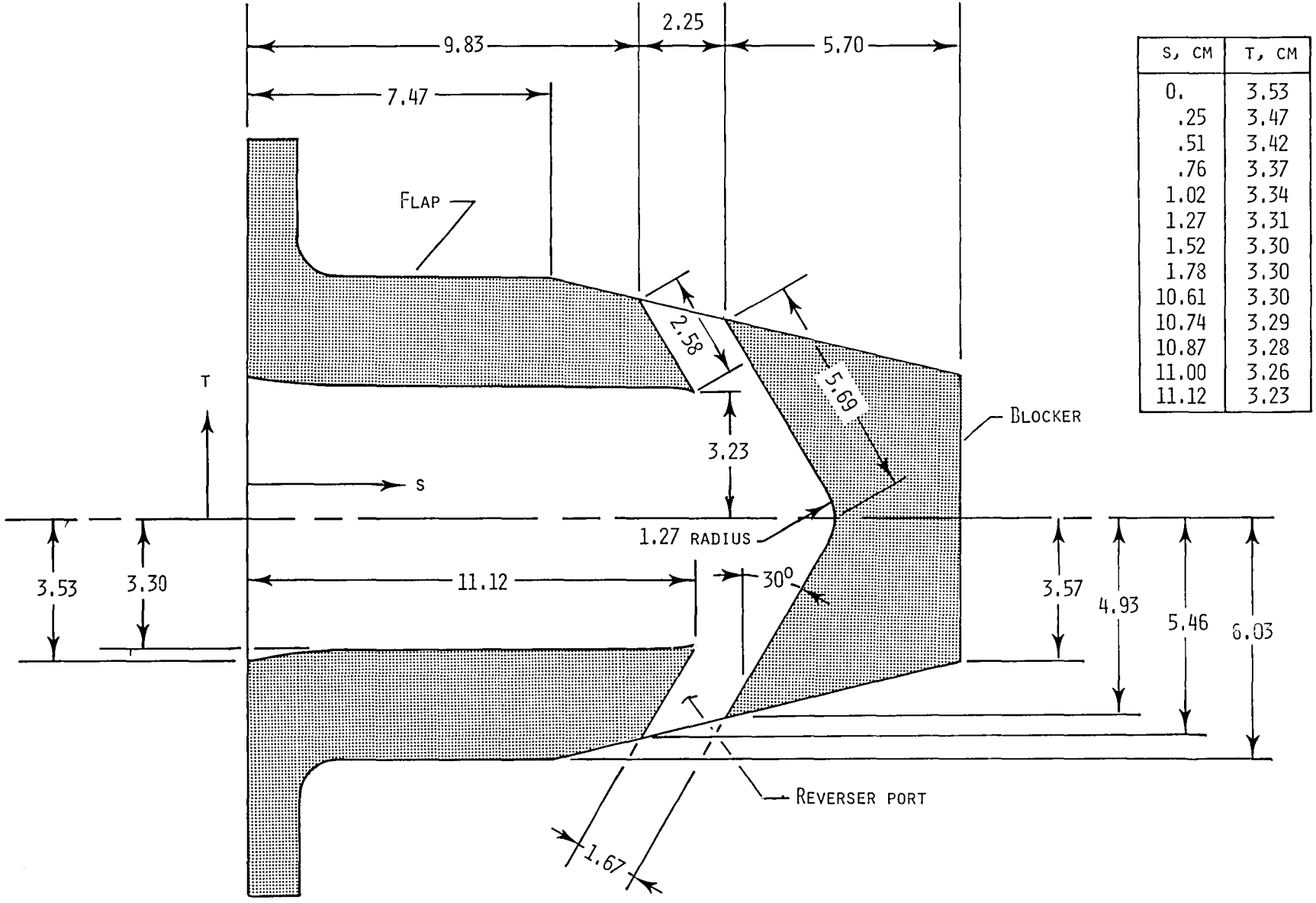

S, CM	T, CM
0.	3.53
.25	3.47
.51	3.42
.76	3.37
1.02	3.34
1.27	3.31
1.52	3.30
1.78	3.30
10.61	3.30
10.74	3.29
10.87	3.28
11.00	3.26
11.12	3.23

Figure 2.- Details of 2-D convergent-divergent thrust-reversing nozzle. Internal width of nozzle is 10.160 cm. All dimensions are in centimeters unless otherwise noted.

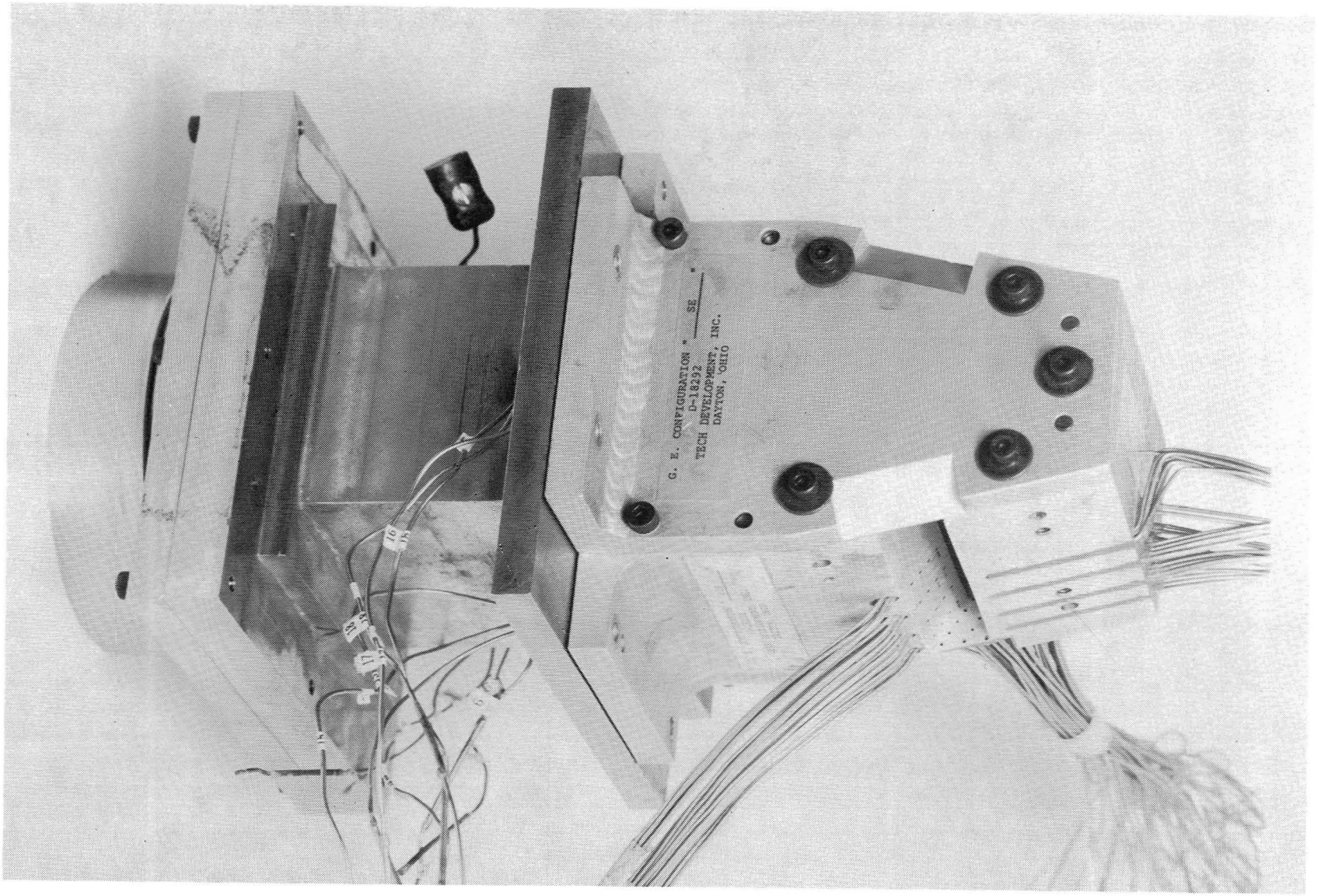

L-83-115

Figure 3.- Photograph of model.

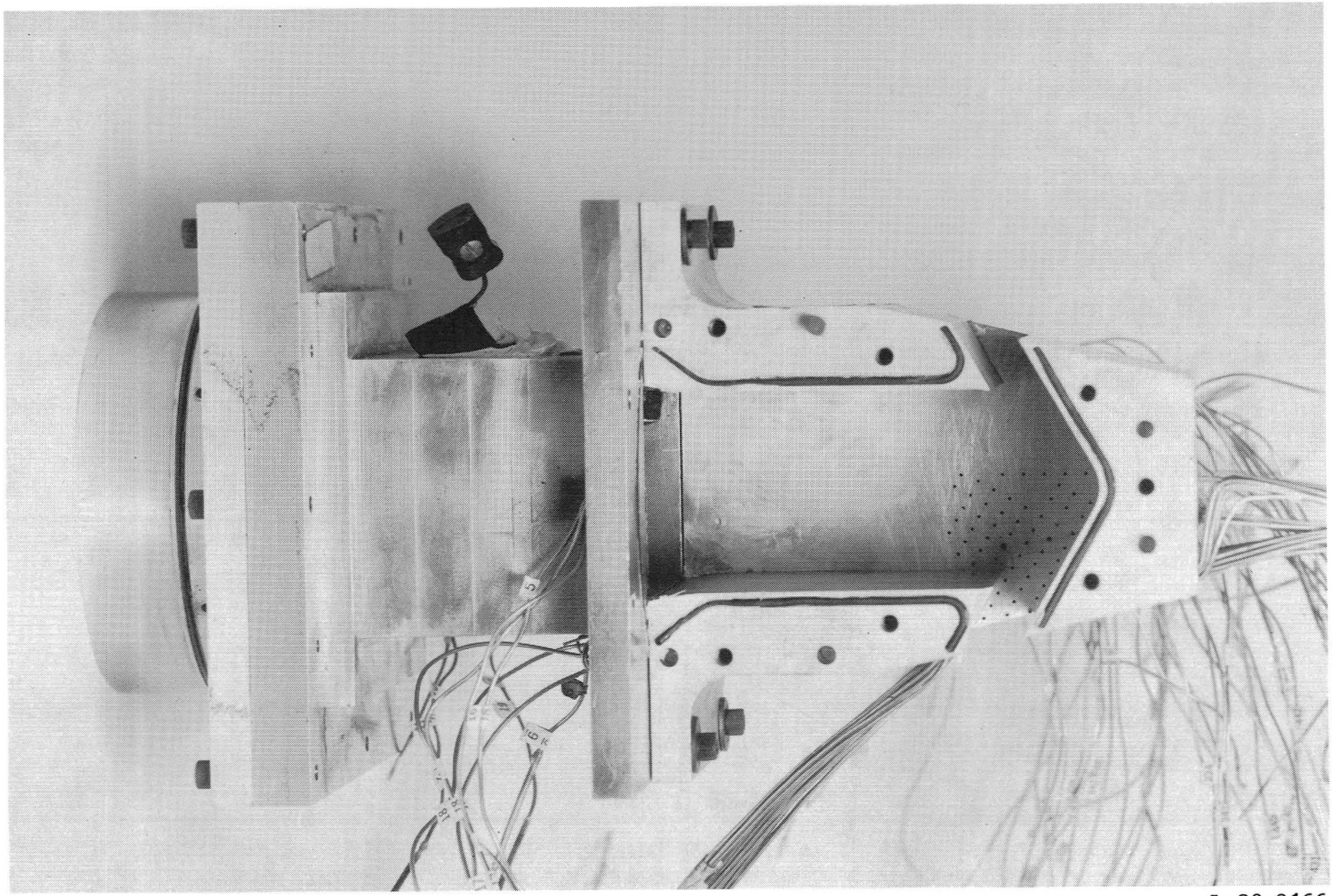

L-82-8166

Figure 4.- Photograph of model with sidewall removed.

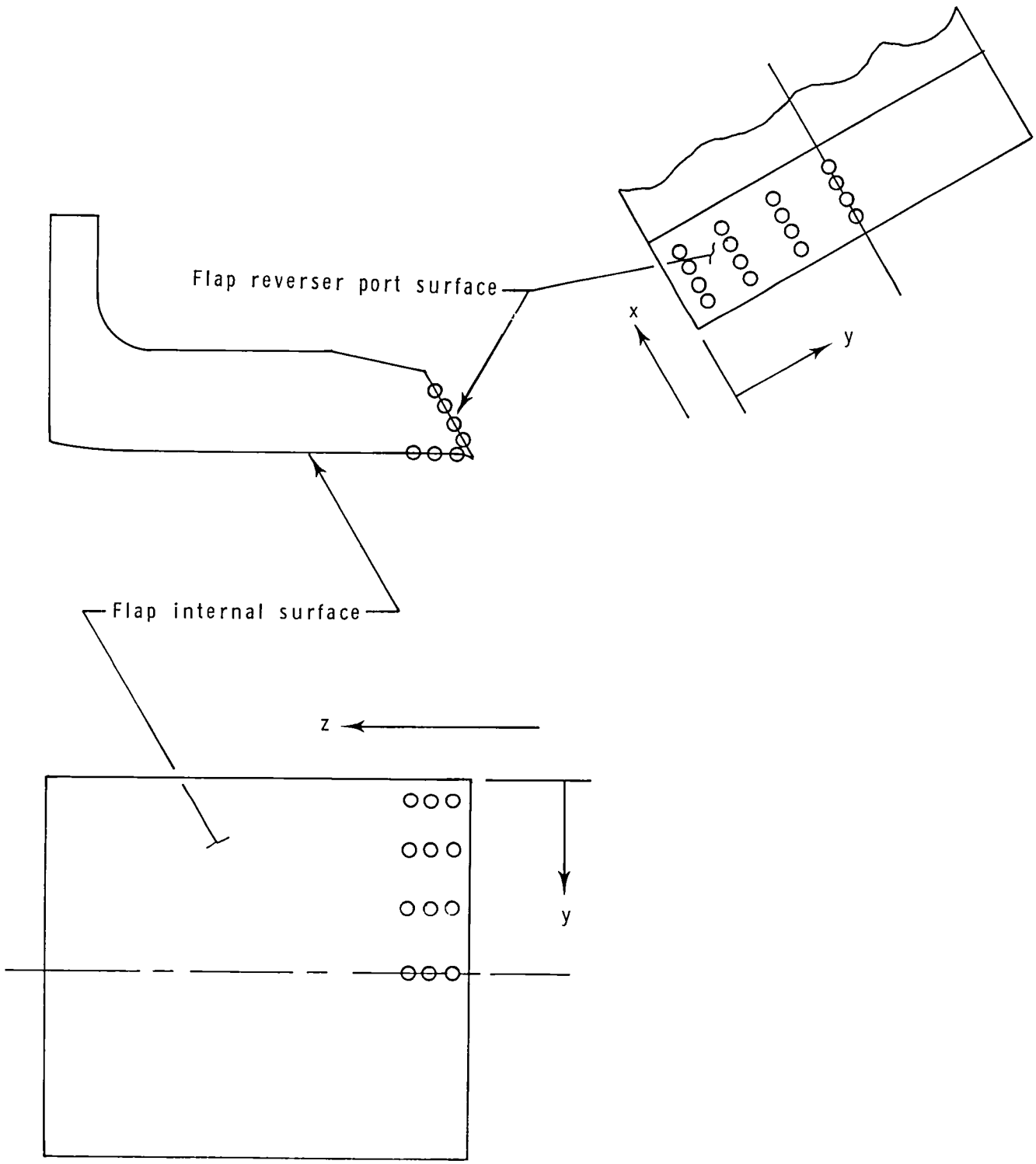

(a) Upper flap.

Figure 5.- Sketches showing typical nozzle internal static-pressure instrumentation. Exact orifice locations are given in table I.

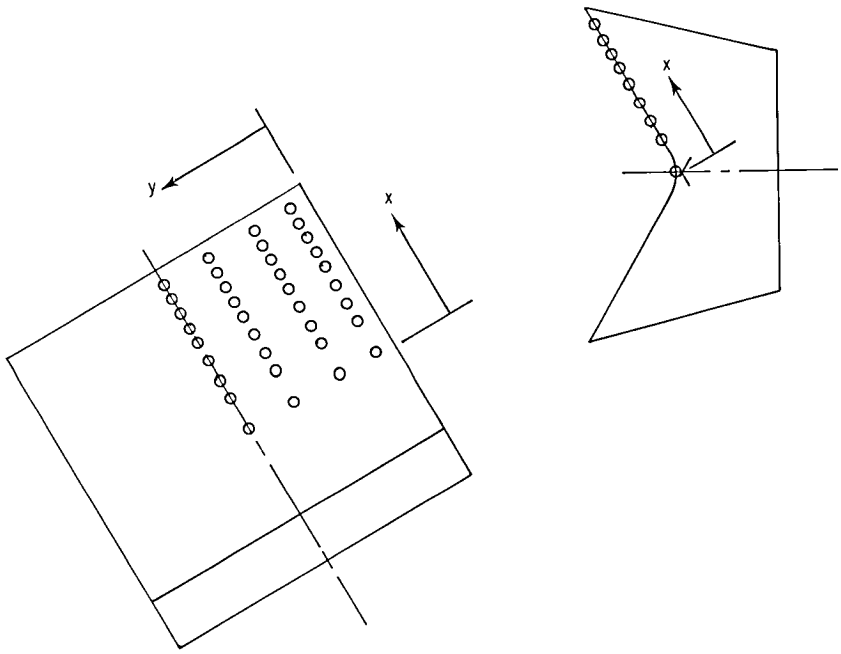

(b) Blocker.

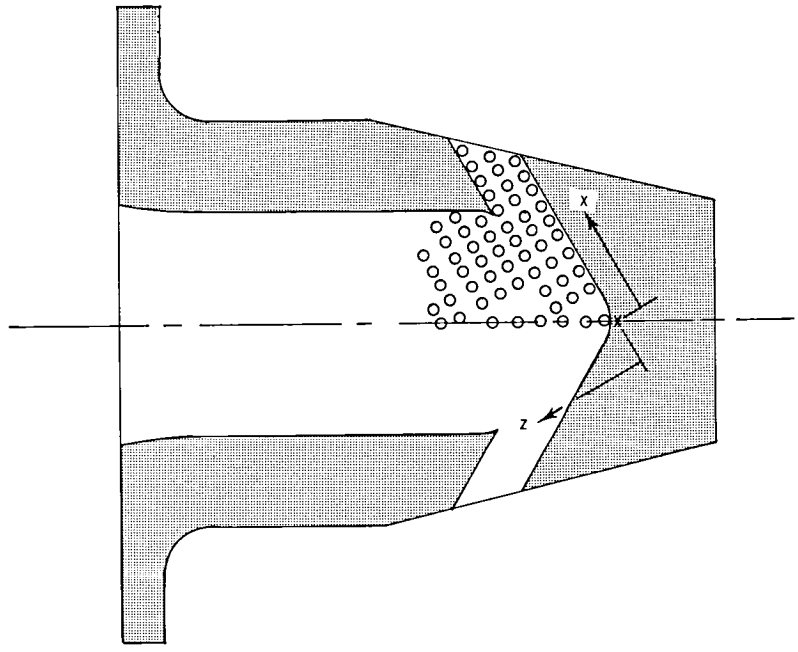

(c) Sidewall.

Figure 5.- Concluded.

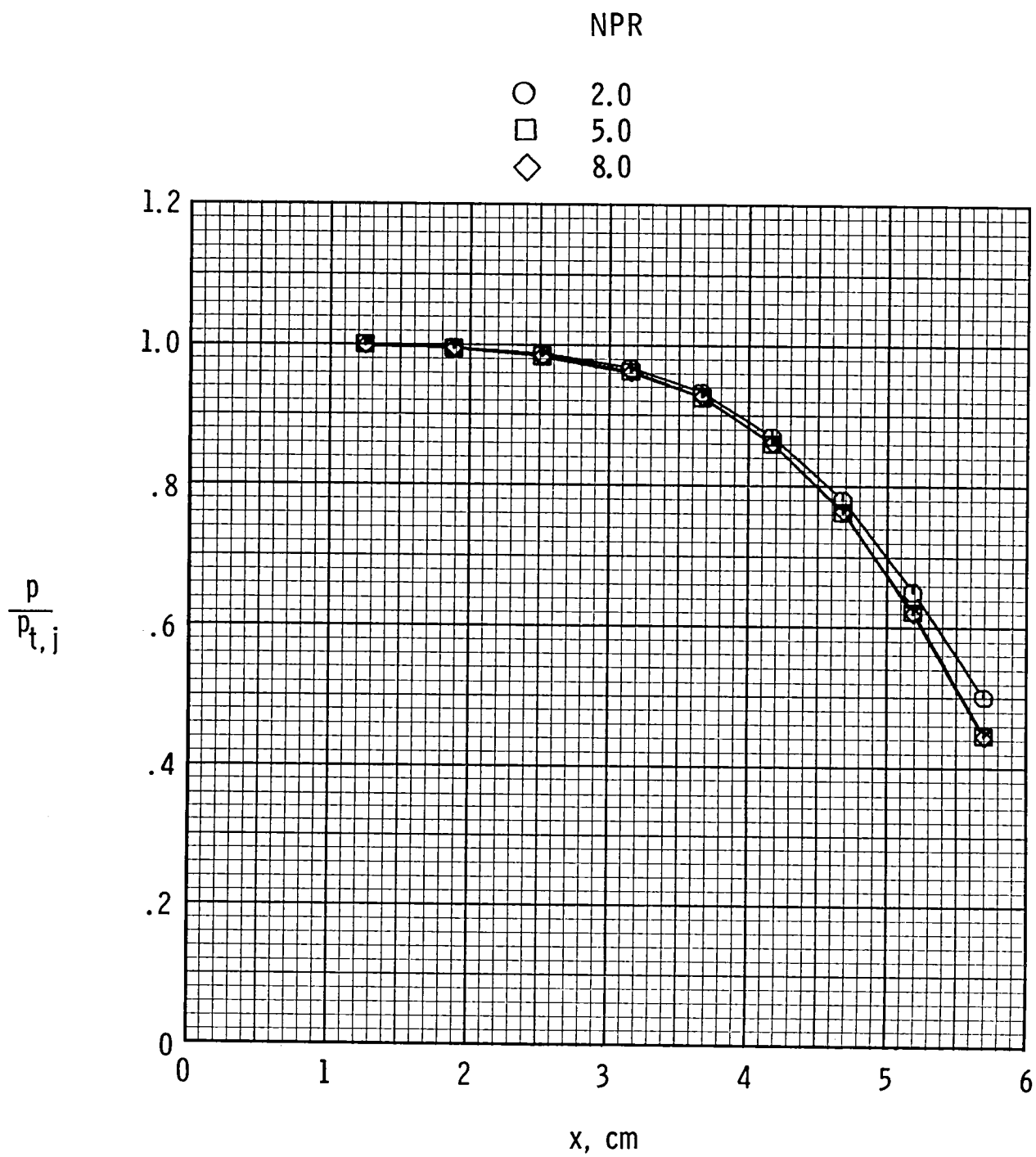

(a) z = 0.203 cm.

Figure 6.- Effect of nozzle pressure ratio on sidewall pressures.

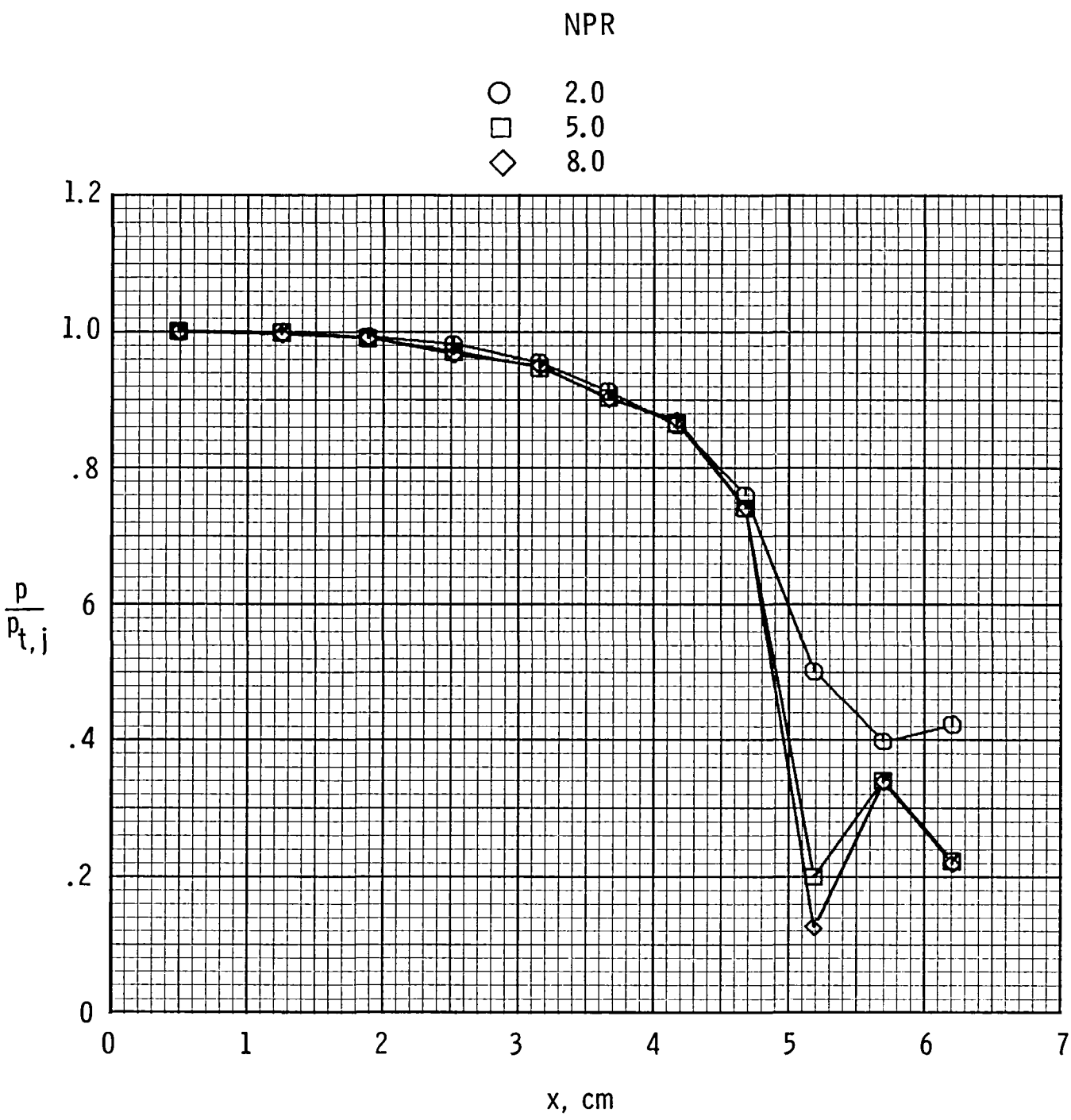

(b) z = 0.828 cm.

Figure 6.- Continued.

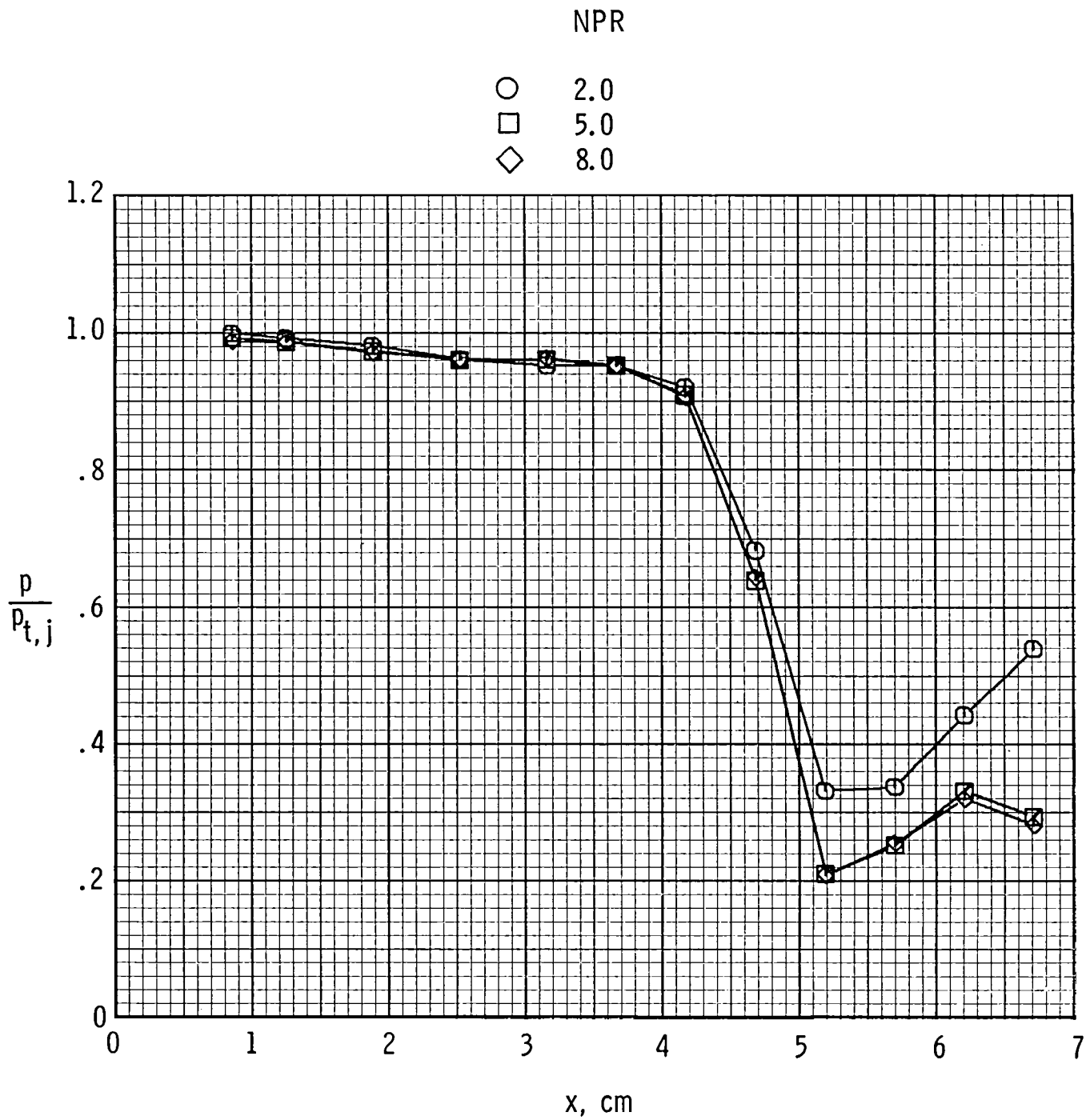

(c) z = 1.473 cm.

Figure 6.- Concluded.

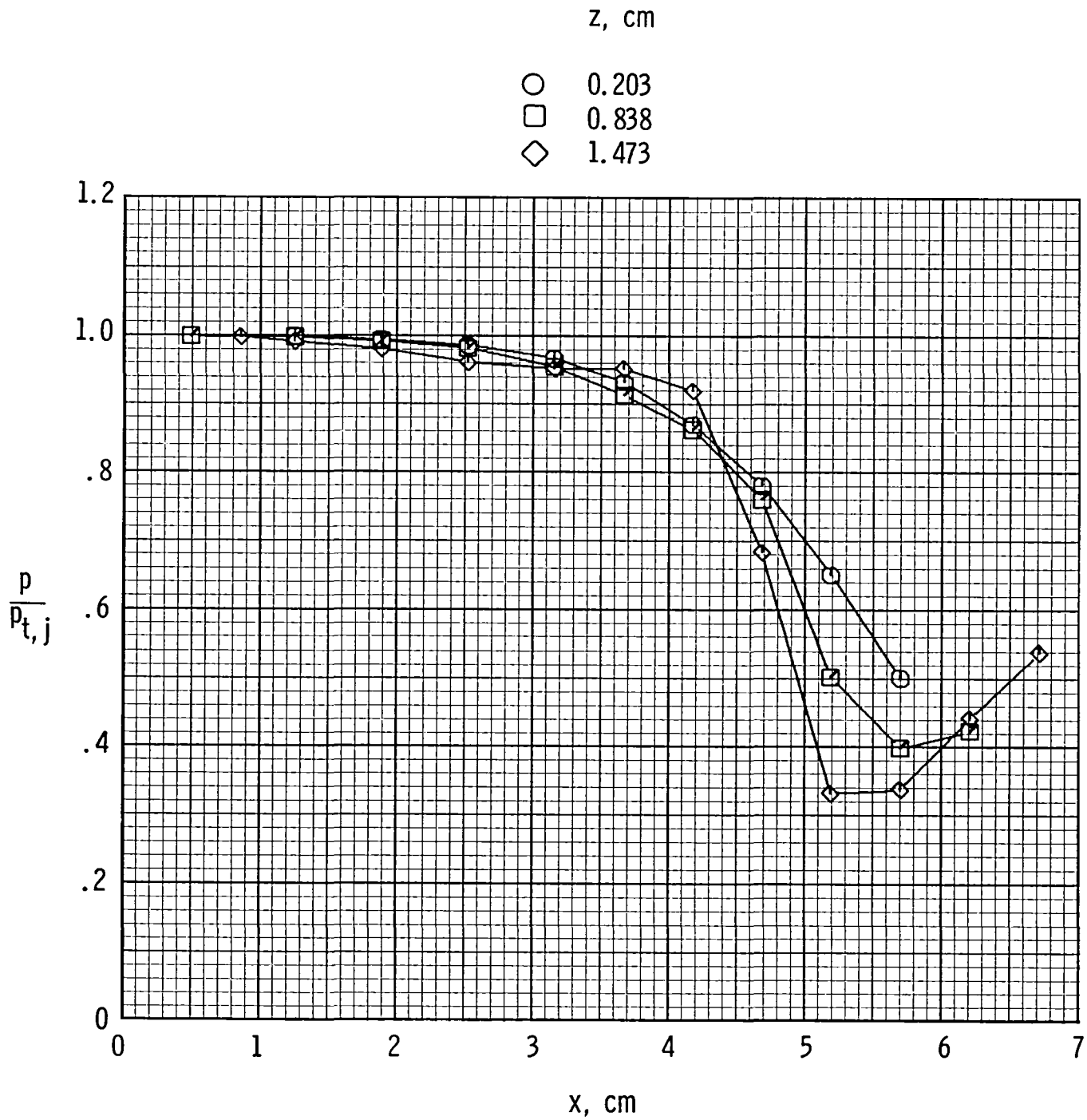

(a) NPR = 2.0.

Figure 7.- Variation of sidewall pressures with x.

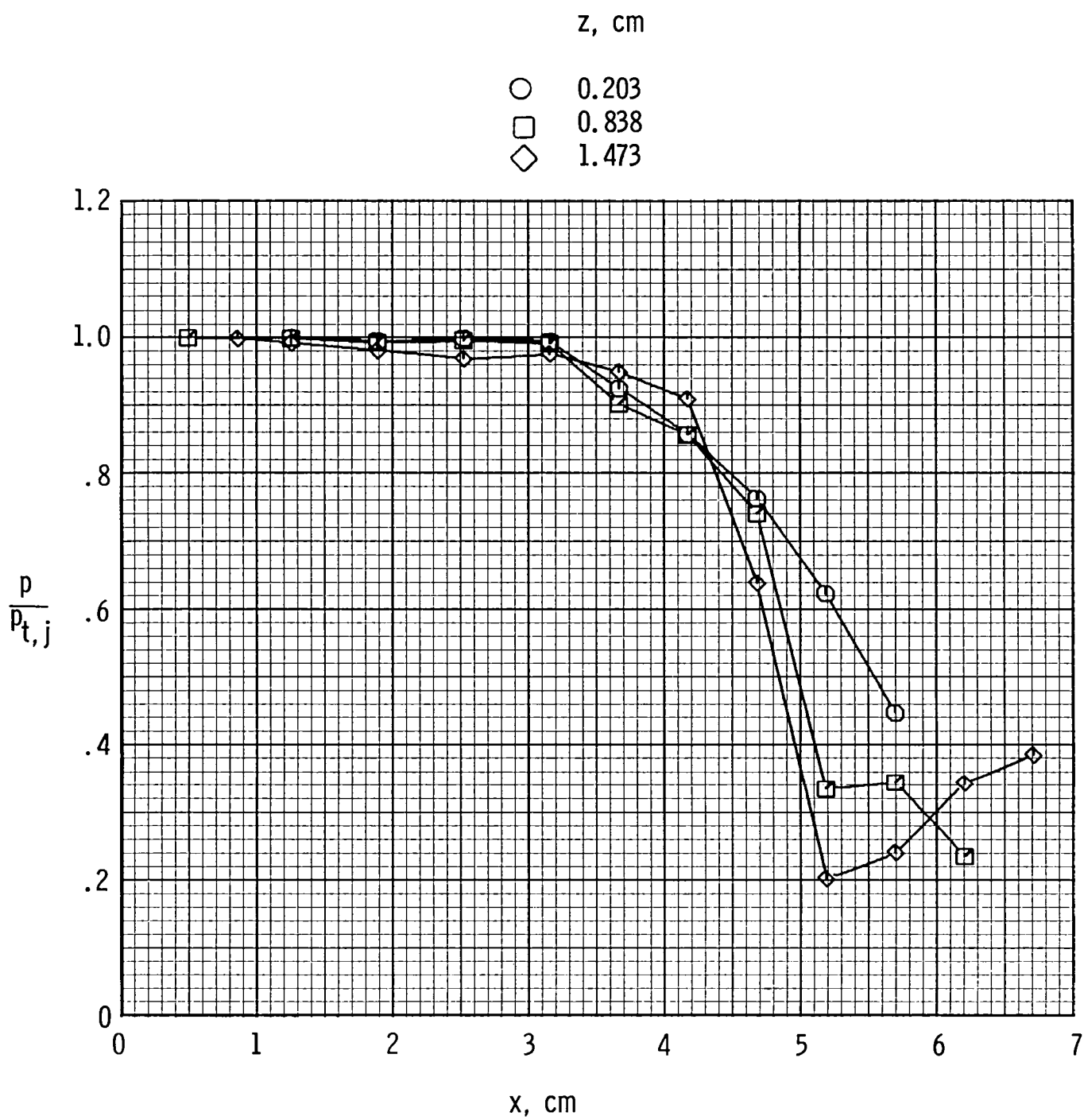

(b) NPR = 3.0.

Figure 7.- Continued.

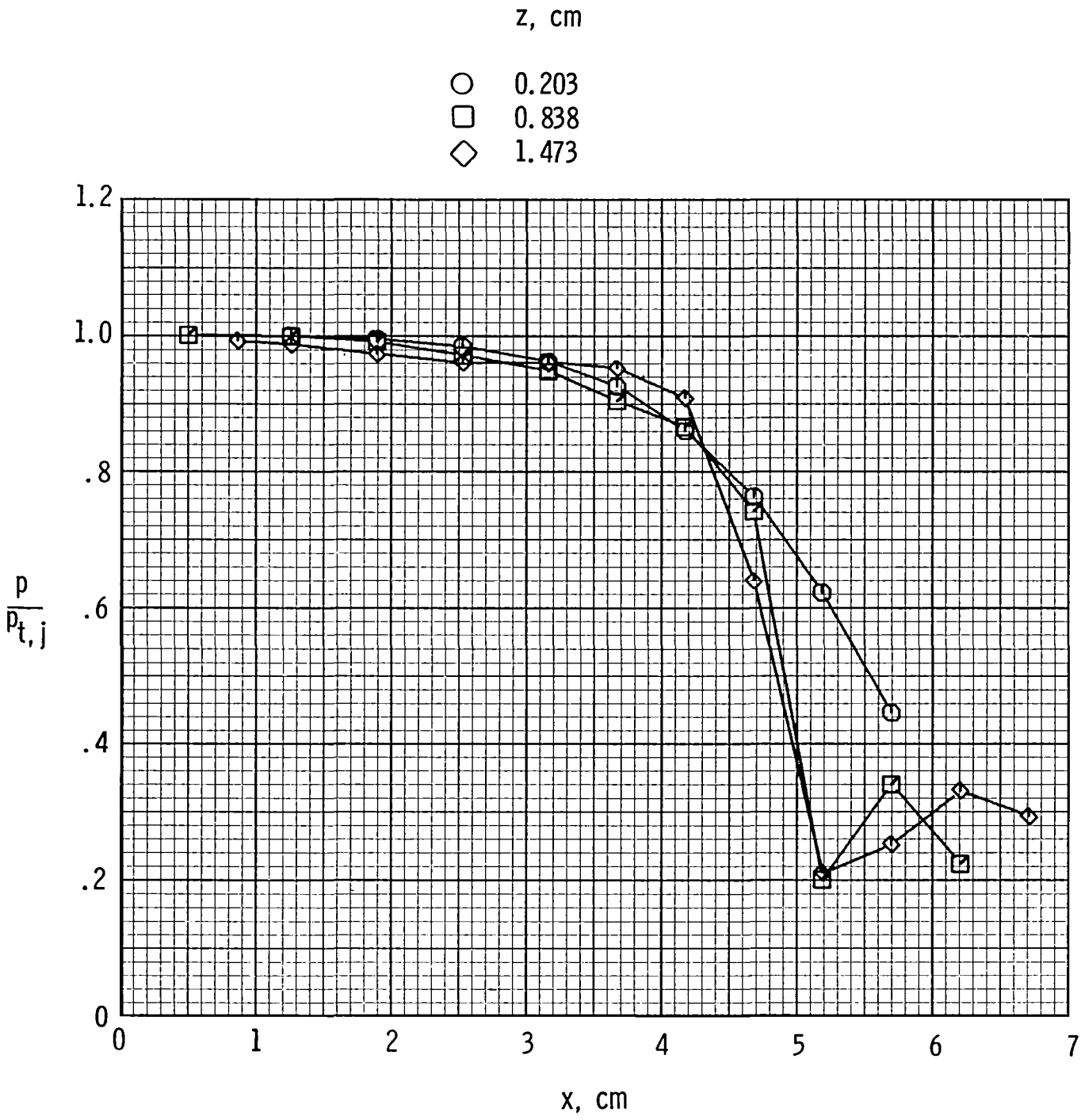

(c) NPR = 5.0.

Figure 7.- Continued.

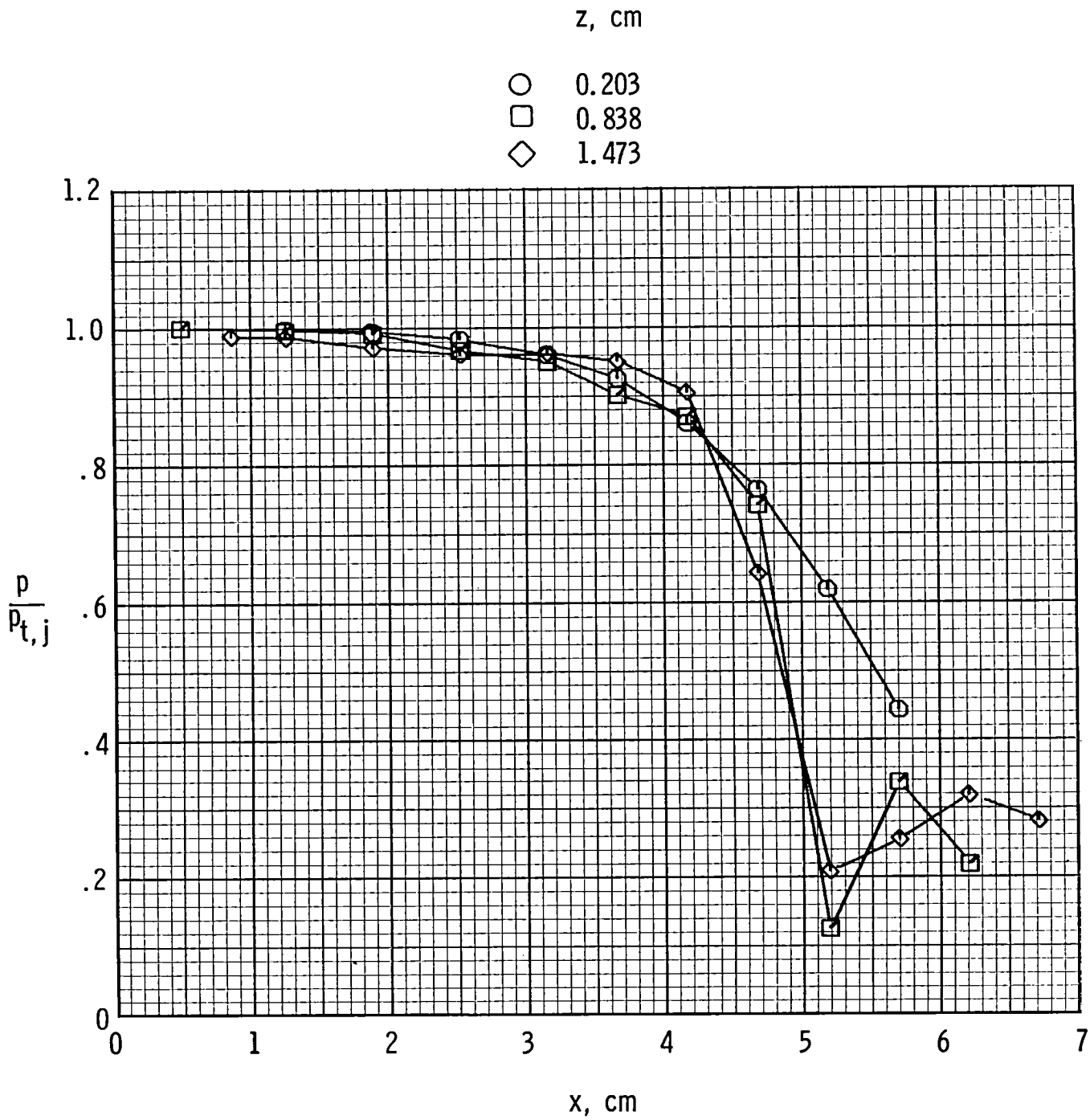

(d) NPR = 8.0.

Figure 7.- Concluded.

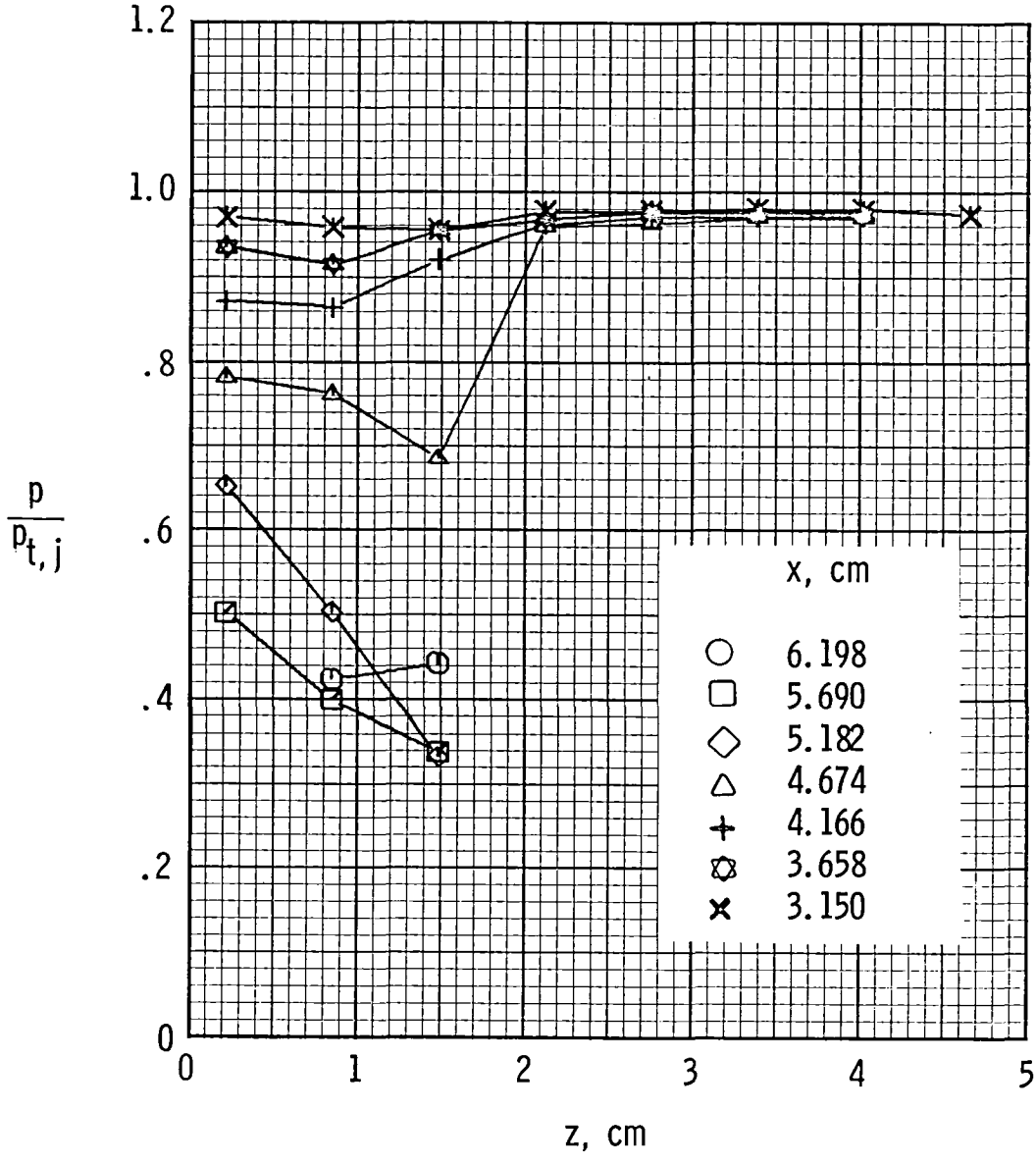

(a) NPR = 2.0.

Figure 8.- Variation of sidewall pressures with z.

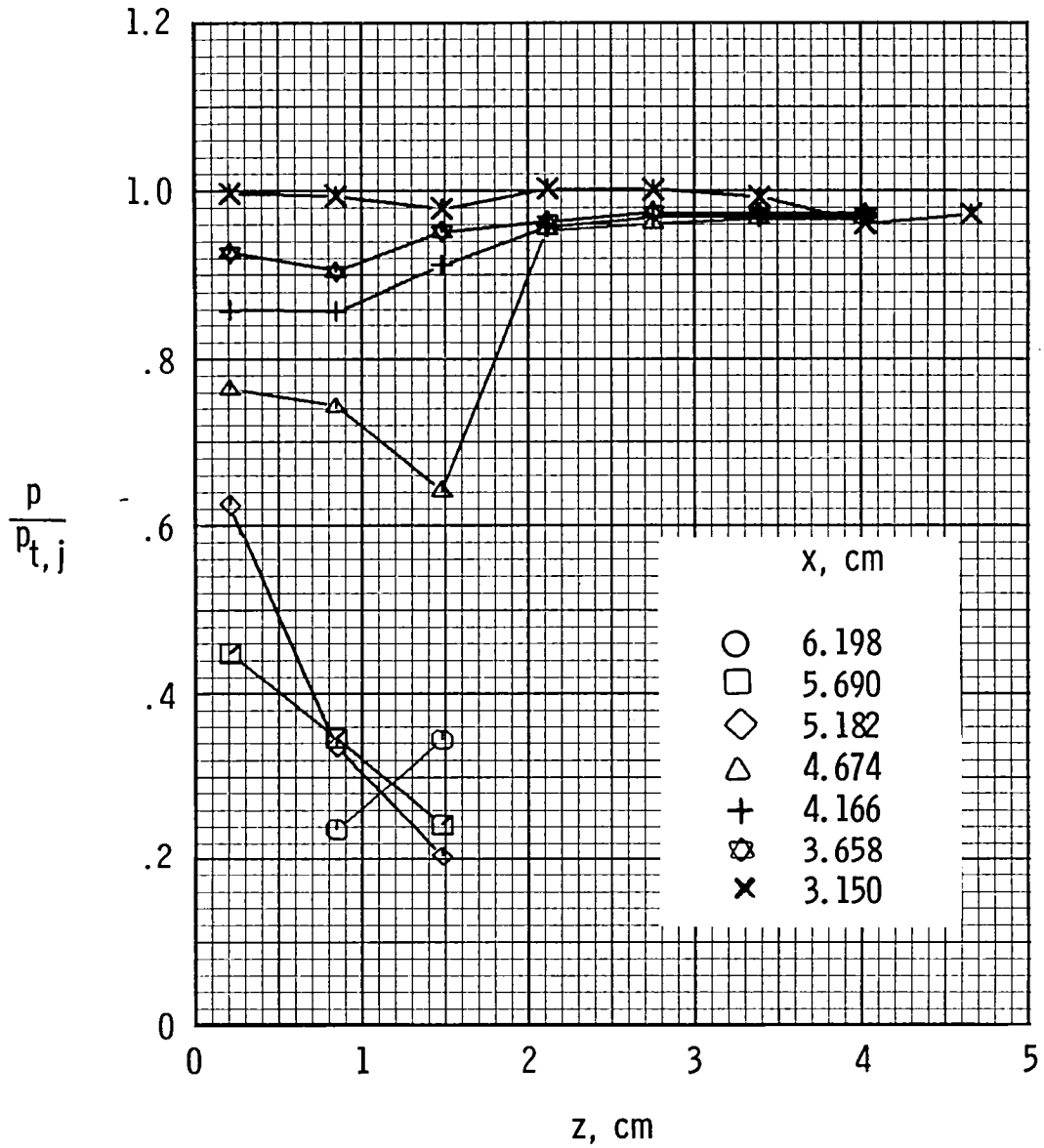

(b) NPR = 3.0.

Figure 8.- Continued.

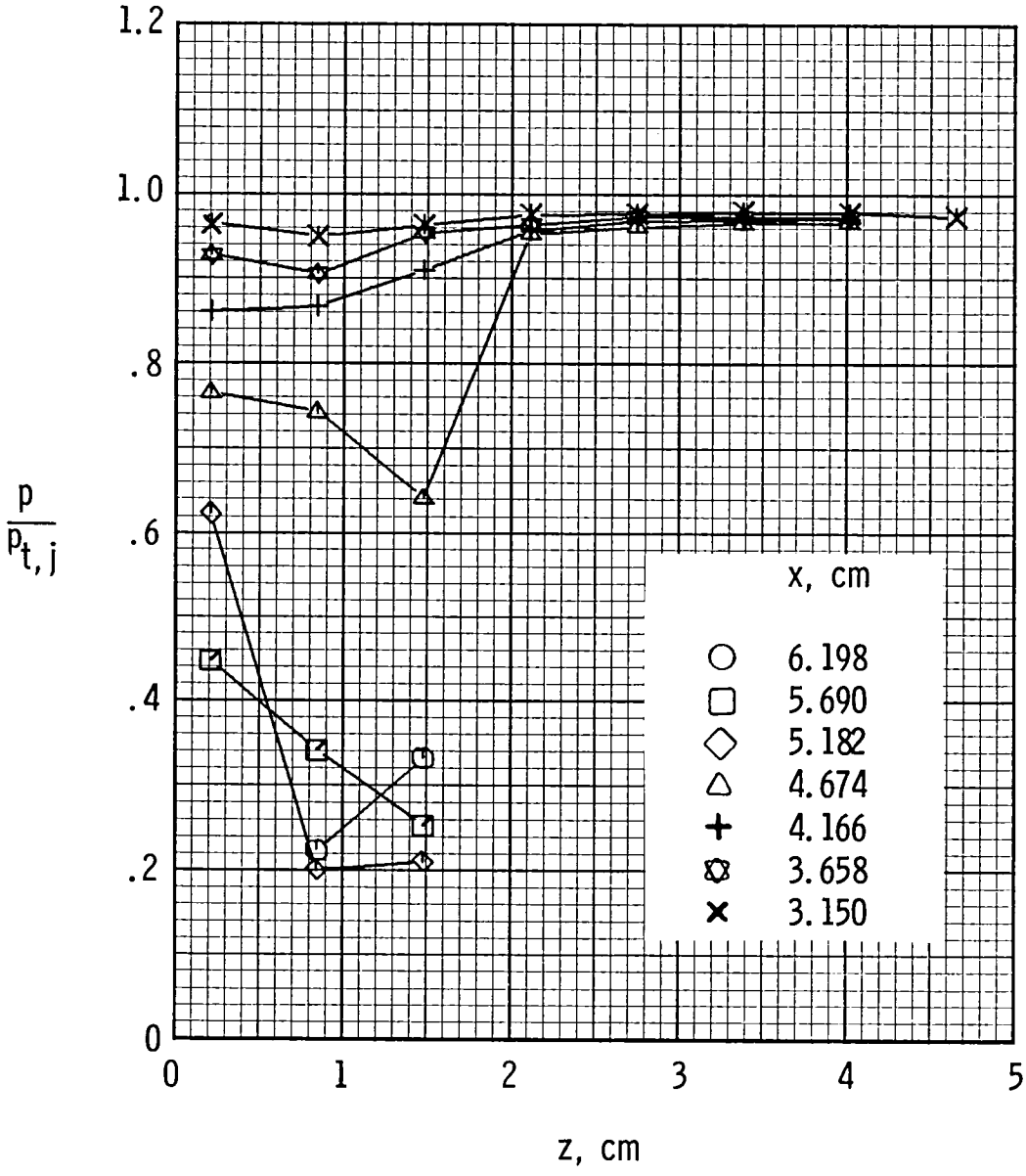

(c) NPR = 5.0.

Figure 8.- Continued.

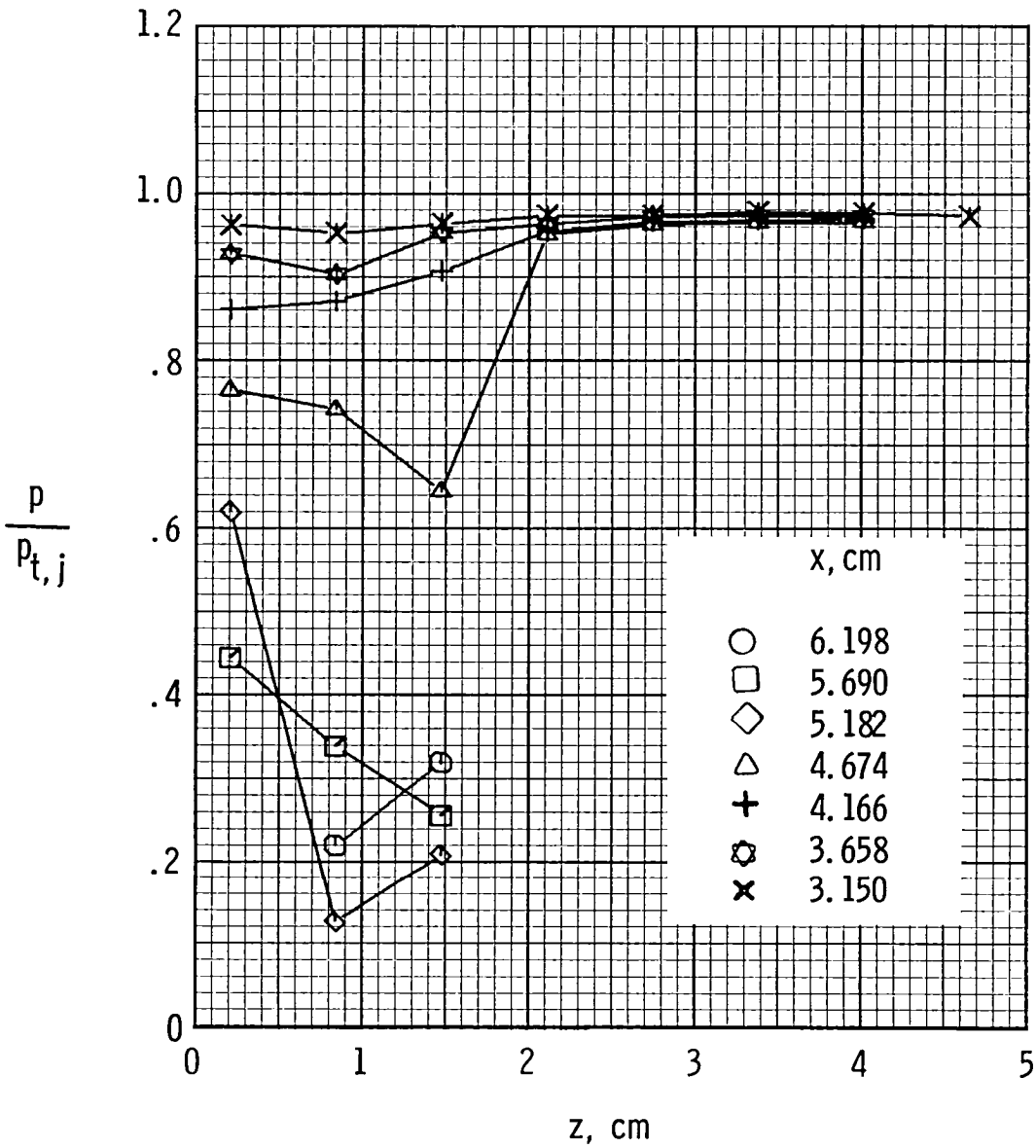

(d) NPR = 8.0.

Figure 8.- Concluded.

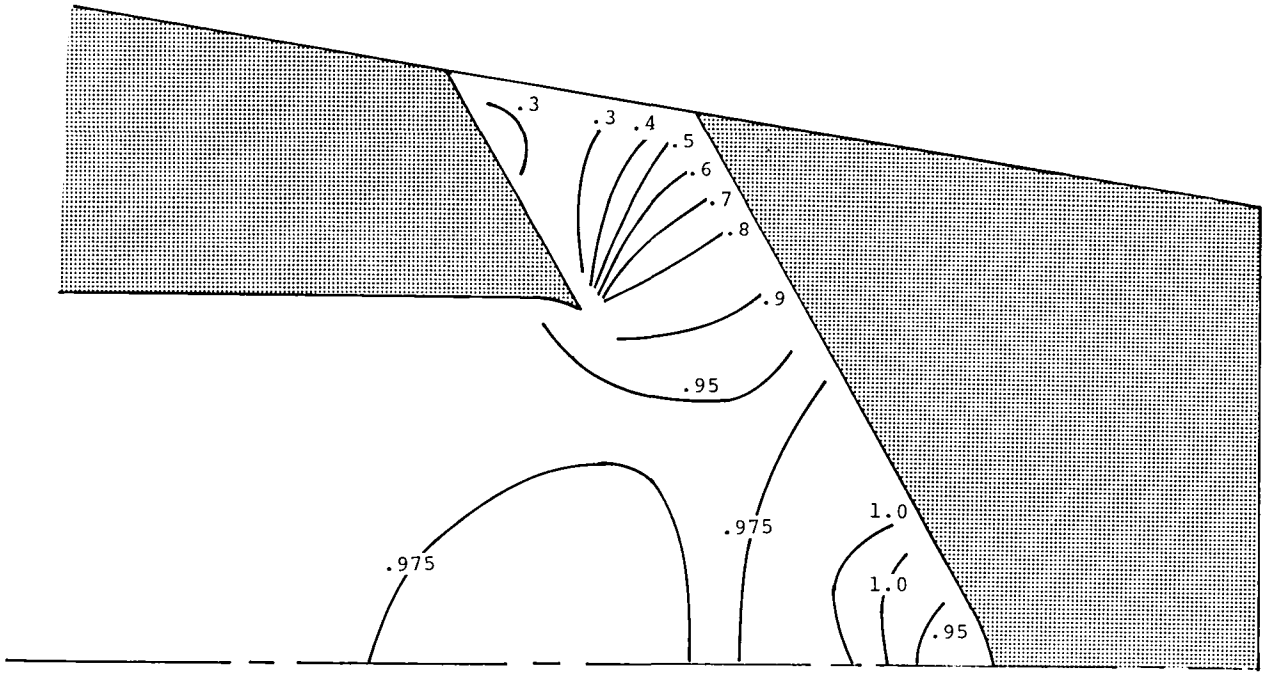

Figure 9.- Contours of $p/p_{t,j}$ on the nozzle sidewall for NPR = 5.0.

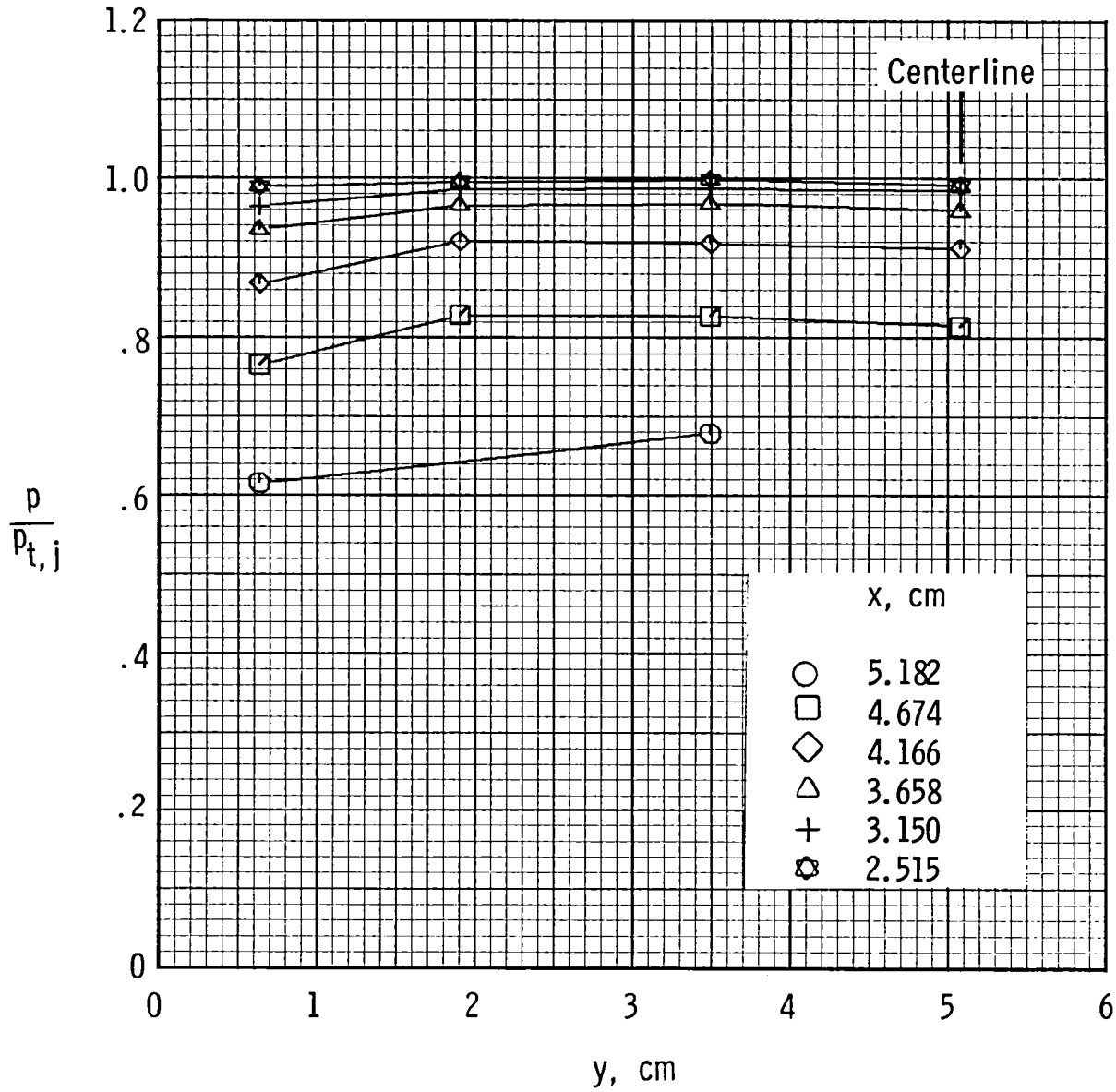

(a) NPR = 2.0.

Figure 10.- Variation of blocker-face pressures with y.

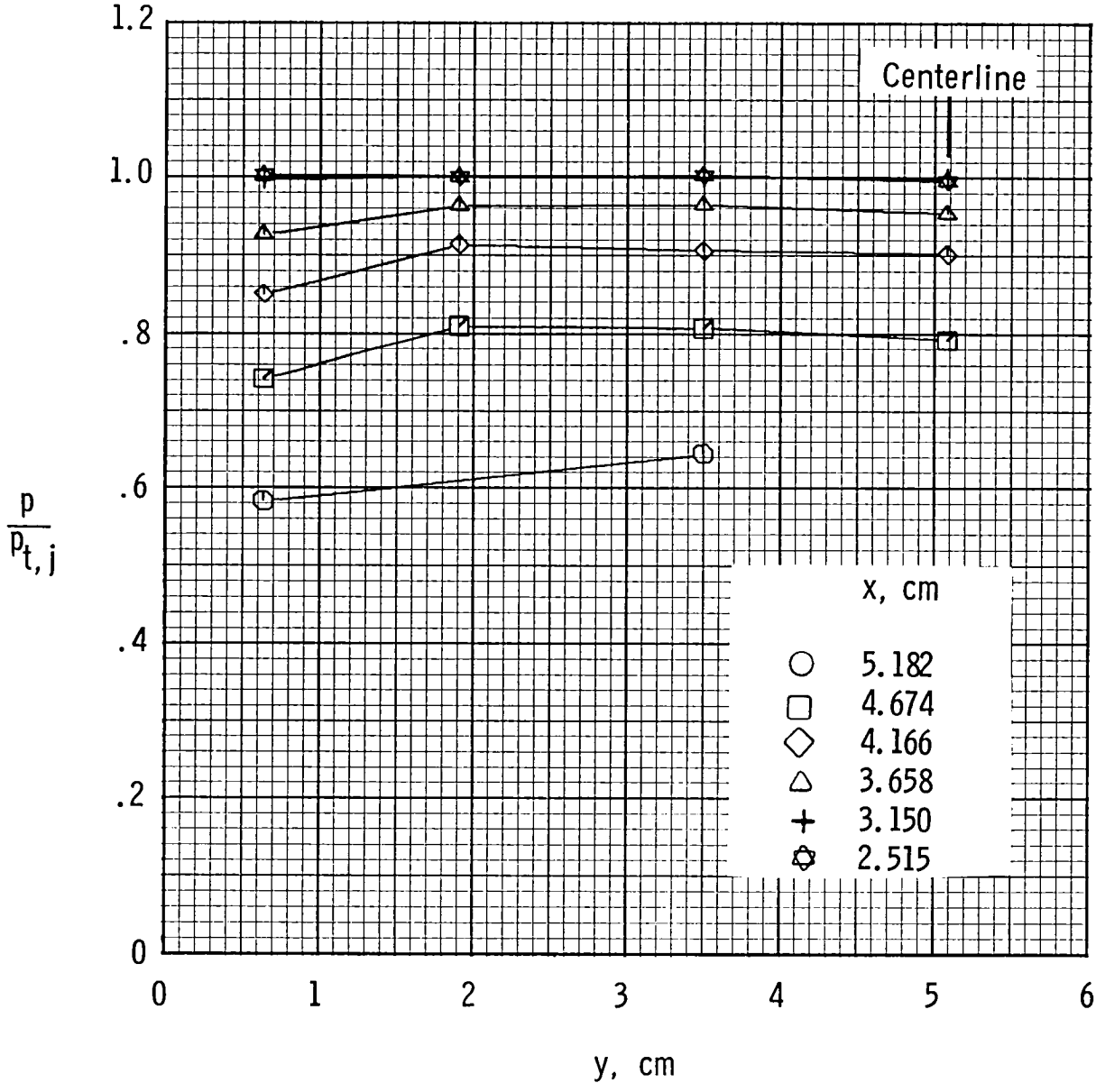

(b) NPR = 3.0.

Figure 10.- Continued.

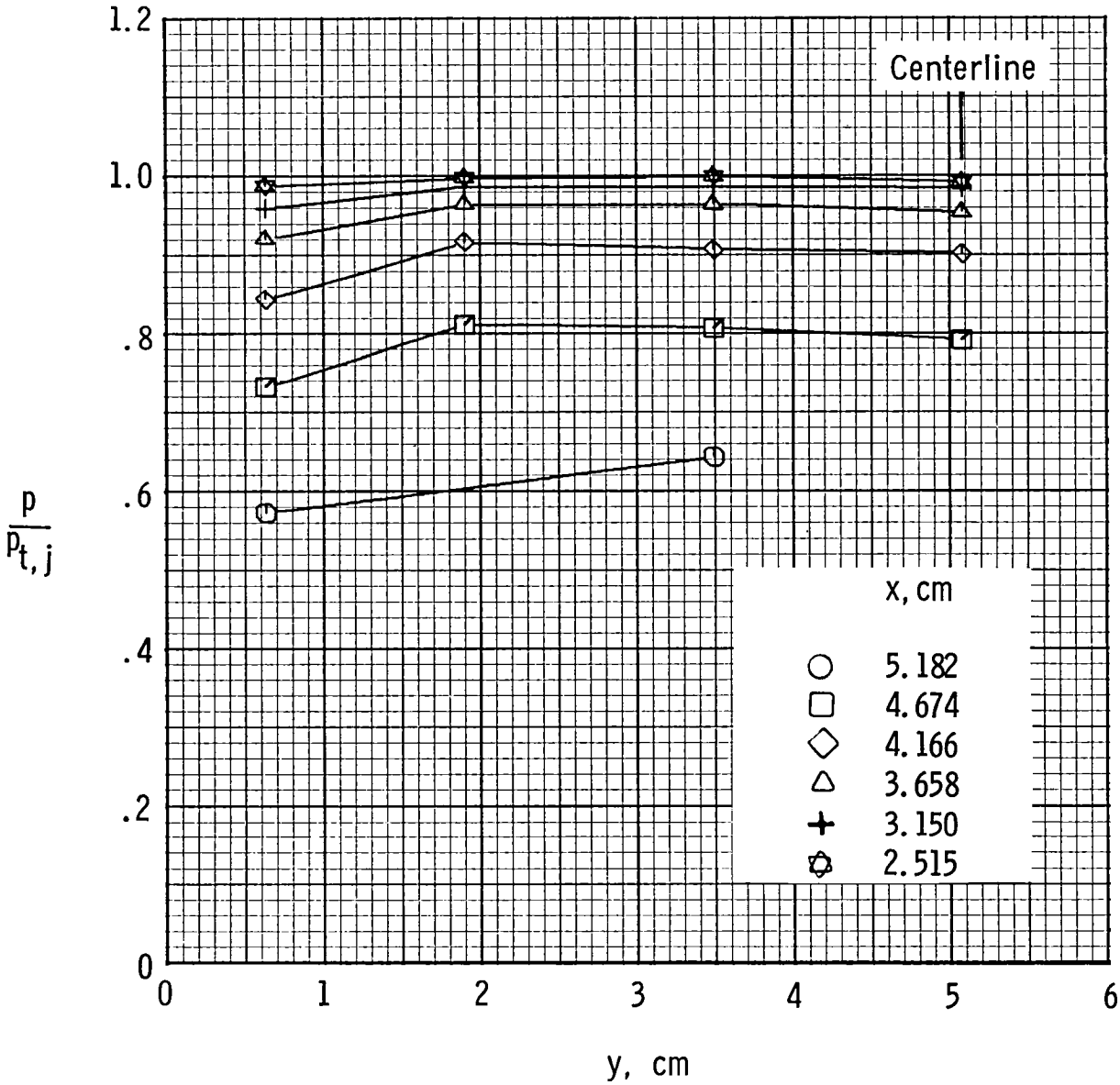

(c) NPR = 5.0.

Figure 10.- Continued.

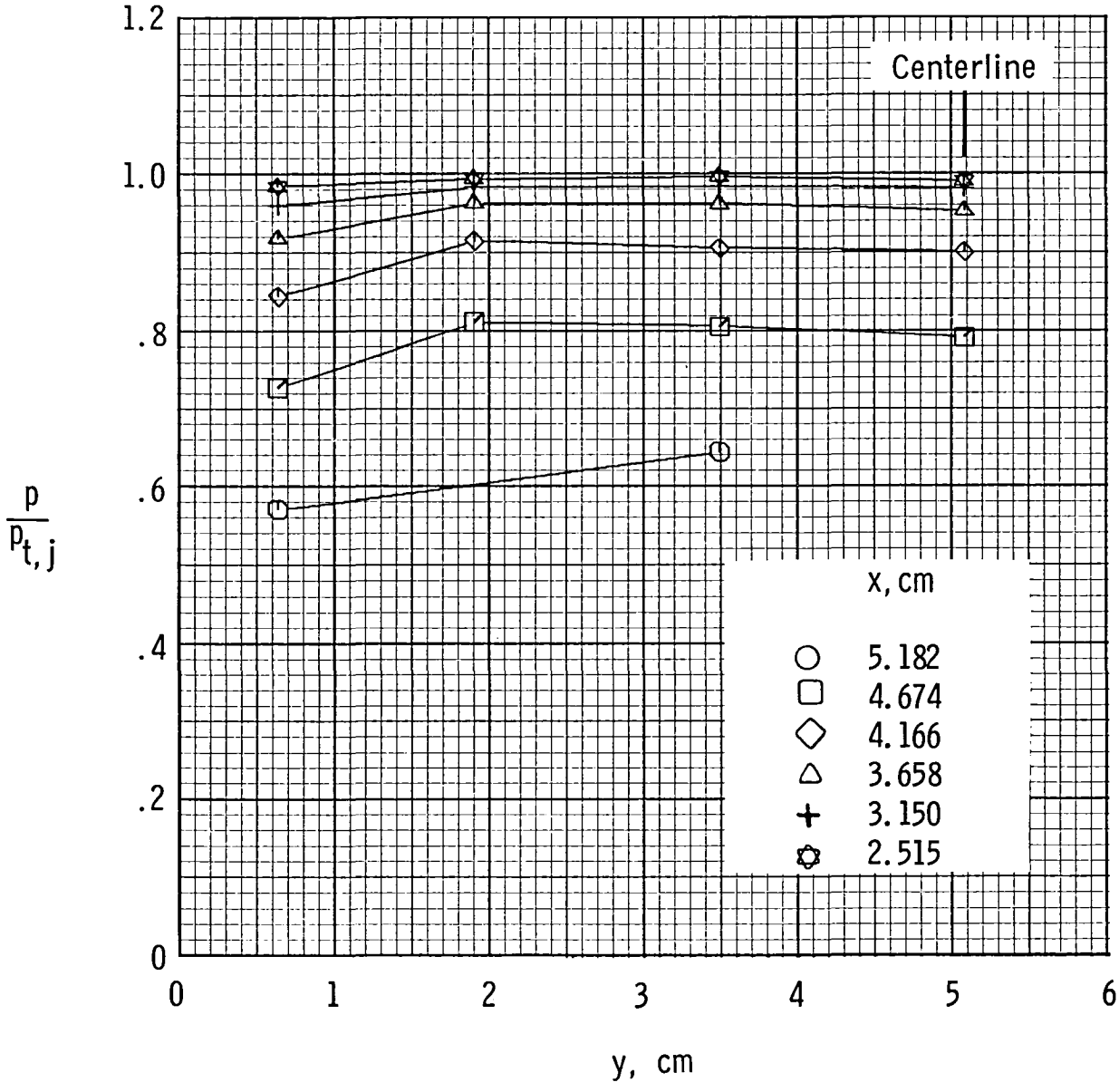

(d) NPR = 8.0.

Figure 10.- Concluded.

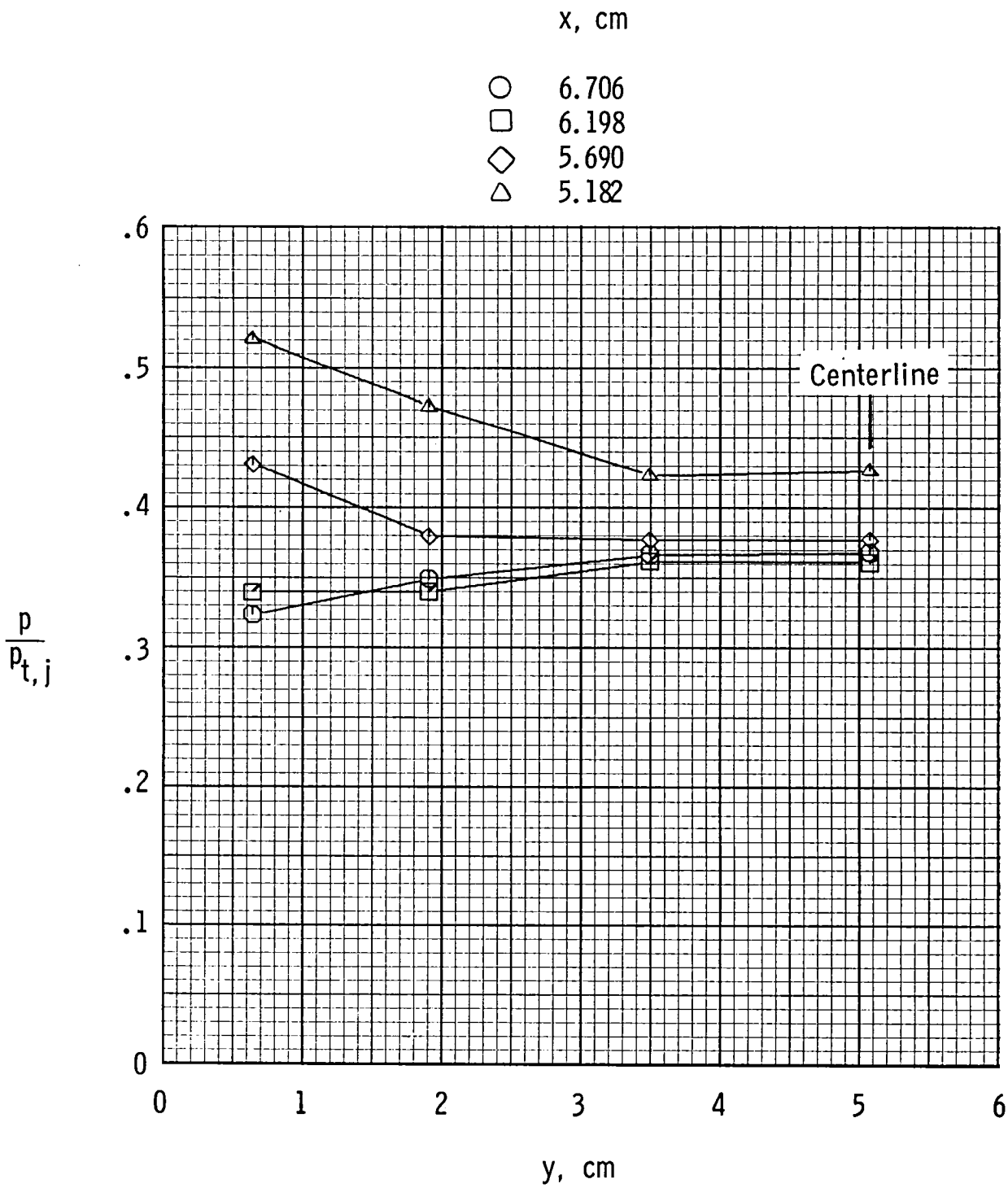

(a) NPR = 2.0.

Figure 11.- Variation of pressures in reverser port on flap with y.

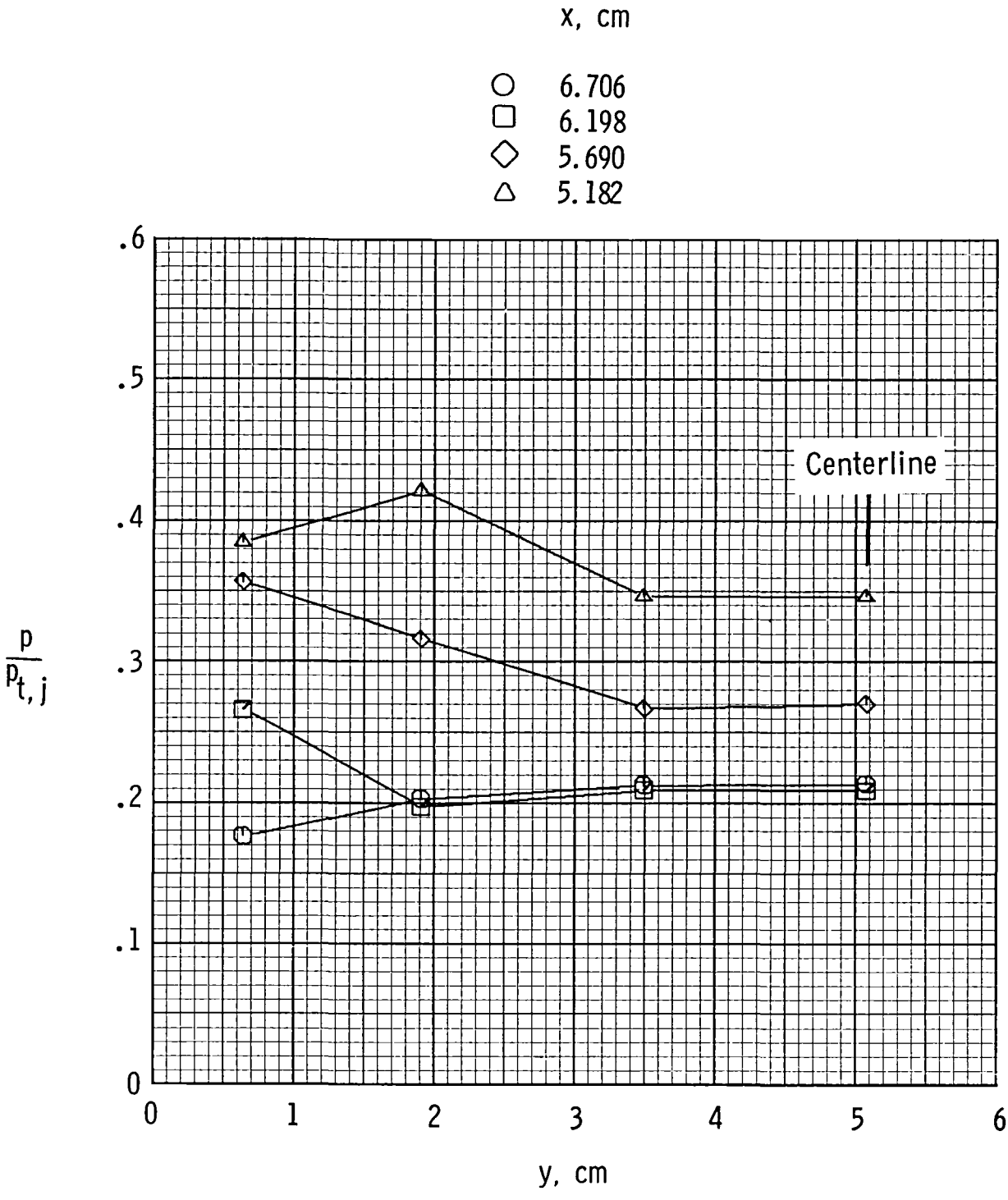

(b) NPR = 3.0.

Figure 11.- Continued.

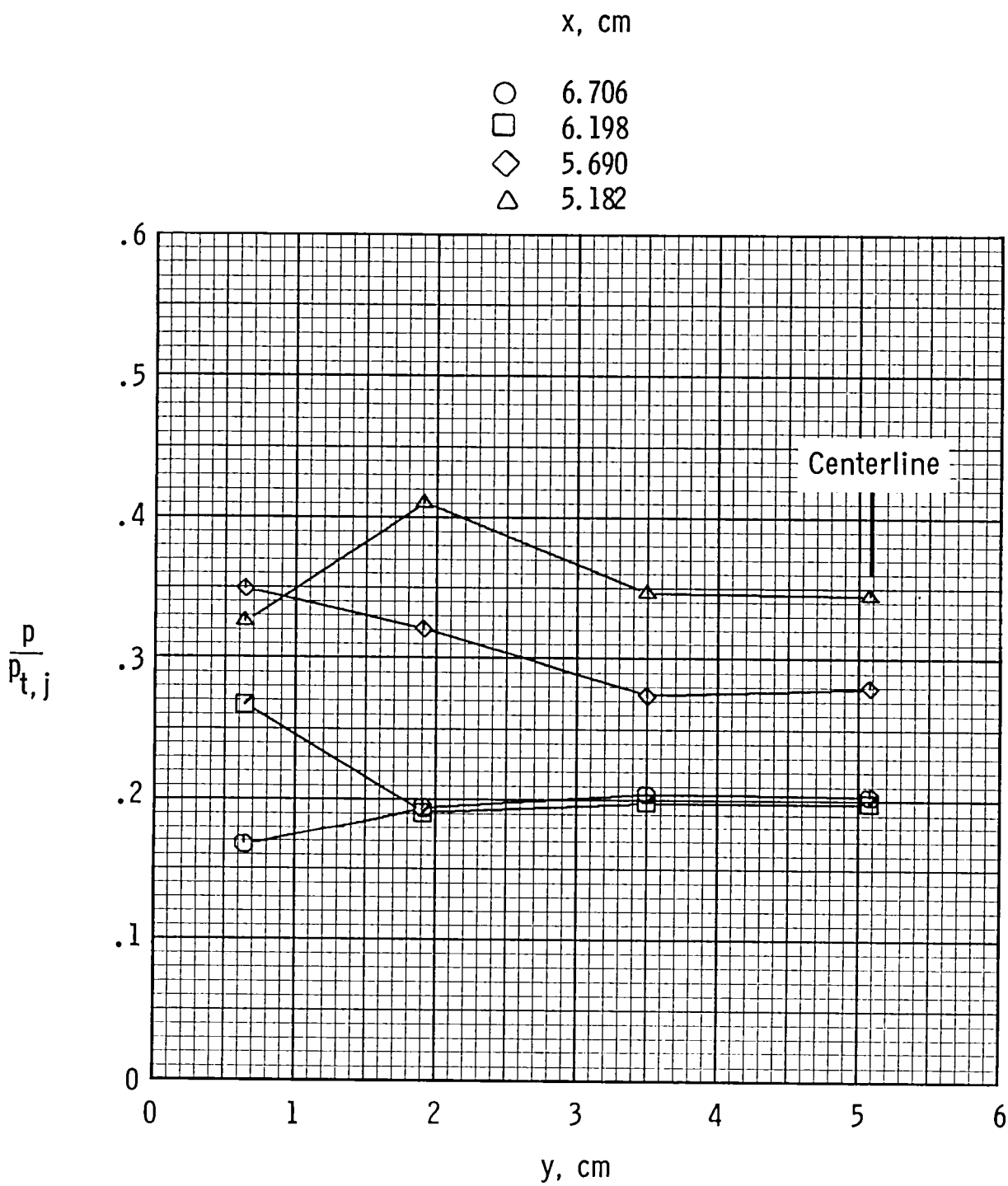

(c) NPR = 5.0.

Figure 11.- Continued.

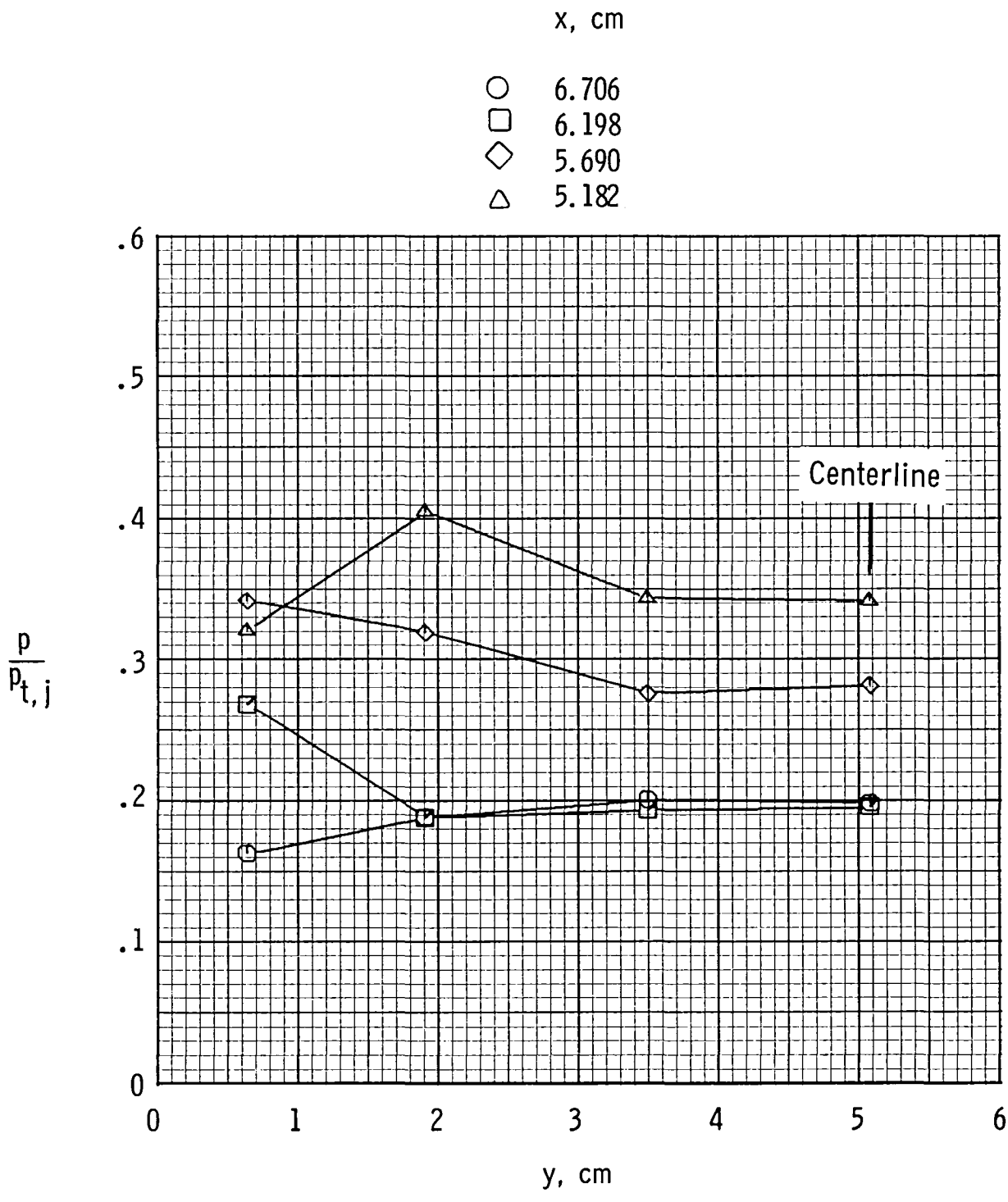

(d) NPR = 8.0.

Figure 11.- Concluded.

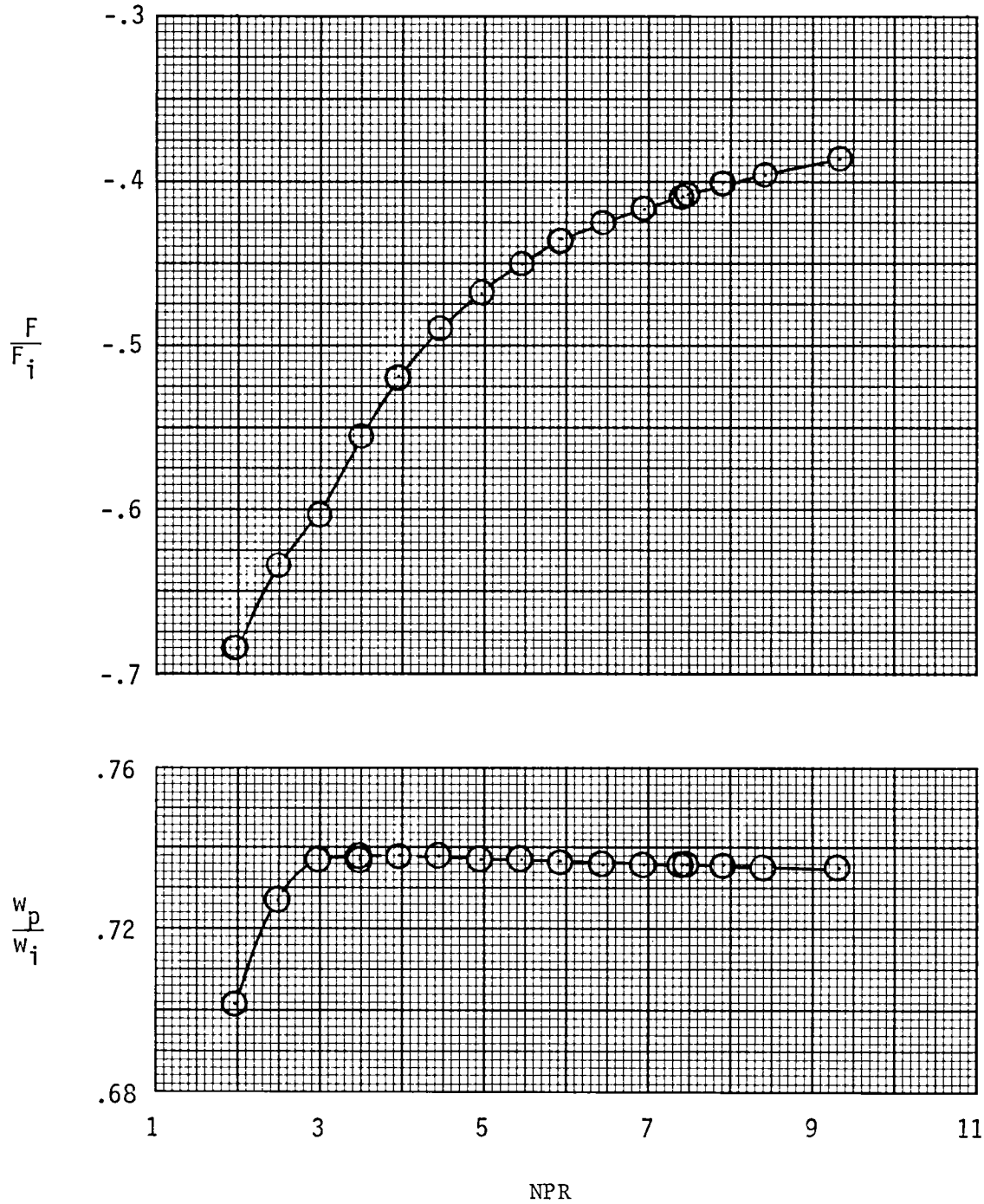

Figure 12.- Thrust and discharge coefficient for the thrust-reversing nozzle from Re and Leavitt (ref. 14).

1. Report No.	2. Government Accession No.	3. Recipient's Catalog No.
NASA TM-85655		

4. Title and Subtitle	5. Report Date
INTERNAL PRESSURE DISTRIBUTIONS FOR A TWO-DIMENSIONAL THRUST-REVERSING NOZZLE OPERATING AT A FREE-STREAM MACH NUMBER OF ZERO	December 1983
	6. Performing Organization Code: 505-31-23-08
7. Author(s): Lawrence E. Putnam and Edward G. Strong	8. Performing Organization Report No.: L-15582
	10. Work Unit No.
9. Performing Organization Name and Address: NASA Langley Research Center, Hampton, VA 23665	11. Contract or Grant No.
	13. Type of Report and Period Covered: Technical Memorandum
12. Sponsoring Agency Name and Address: National Aeronautics and Space Administration, Washington, DC 20546	14. Sponsoring Agency Code

15. Supplementary Notes

Edward G. Strong was a co-op student from the University of Cincinnati.

16. Abstract

An investigation has been conducted in the static-test facility of the Langley 16-Foot Transonic Tunnel to measure static-pressure distributions inside a nonaxisymmetric thrust-reversing nozzle. The tests were made at nozzle total pressures ranging from ambient to about eight times ambient pressure at a free-stream Mach number of zero. Tabulated pressure data are presented.

17. Key Words (Suggested by Author(s))	18. Distribution Statement
Two-dimensional nozzles Thrust reversing Internal pressures	Unclassified - Unlimited Subject Category 02

19. Security Classif. (of this report)	20. Security Classif. (of this page)	21. No. of Pages	22. Price
Unclassified	Unclassified	43	A03

For sale by the National Technical Information Service, Springfield, Virginia 22161

NASA-Langley, 1983

National Aeronautics and
Space Administration

Washington, D.C.
20546

Official Business
Penalty for Private Use, $300

THIRD-CLASS BULK RATE

Postage and Fees Paid
National Aeronautics and
Space Administration
NASA-451

POSTMASTER: If Undeliverable (Section 158 Postal Manual) Do Not Return